Title

Structure of a Ca2+/CaM:Kv7.4 (KCNQ4) B-Helix Complex Provides Insight into M Current Modulation

Journal

Journal of Molecular Biology, 425(2)

ISSN

0022-2836

Authors

Xu, Qiang
Chang, Aram
Tolia, Alexandra
et al.

Publication Date

2013

DOI

10.1016/j.jmb.2012.11.023

Peer reviewed

jmb Article

Structure of a Ca^{2+}/CaM:Kv7.4 (KCNQ4) B-Helix Complex Provides Insight into M Current Modulation

Qiang Xu[1]†, Aram Chang[1]†, Alexandra Tolia[1] and Daniel L. Minor Jr.[1,2,3,4]

*1 - **Cardiovascular Research Institute,** University of California, San Francisco, CA 94158-2156, USA*
*2 - **Departments of Biochemistry and Biophysics,** and Cellular and Molecular Pharmacology, University of California, San Francisco, CA 94158-2156, USA*
*3 - **California Institute for Quantitative Biosciences,** University of California, San Francisco, CA 94158-2156, USA*
*4 - **Physical Biosciences Division,** Lawrence Berkeley National Laboratory, Berkeley, CA 94720, USA*

Correspondence to Daniel L. Minor: *daniel.minor@ucsf.edu*
http://dx.doi.org/10.1016/j.jmb.2012.11.023
Edited by J. Bowie

Abstract

Calmodulin (CaM) is an important regulator of Kv7.x (KCNQx) voltage-gated potassium channels. Channels from this family produce neuronal M currents and cardiac and auditory I_{KS} currents and harbor mutations that cause arrhythmias, epilepsy, and deafness. Despite extensive functional characterization, biochemical and structural details of the interaction between CaM and the channel have remained elusive. Here, we show that both apo-CaM and Ca^{2+}/CaM bind to the C-terminal tail of the neuronal channel Kv7.4 (KCNQ4), which is involved in both hearing and mechanosensation. Interactions between apo-CaM and the Kv7.4 tail involve two C-terminal tail segments, known as the A and B segments, whereas the interaction between Ca^{2+}/CaM and the Kv7.4 C-terminal tail requires only the B segment. Biochemical studies show that the calcium dependence of the CaM:B segment interaction is conserved in all Kv7 subtypes. X-ray crystallographic determination of the structure of the Ca^{2+}/CaM:Kv7.4 B segment complex shows that Ca^{2+}/CaM wraps around the Kv7.4 B segment, which forms an α-helix, in an antiparallel orientation that embodies a variation of the classic 1-14 Ca^{2+}/CaM interaction motif. Taken together with the context of prior studies, our data suggest a model for modulation of neuronal Kv7 channels involving a calcium-dependent conformational switch from an apo-CaM form that bridges the A and B segments to a Ca^{2+}/CaM form bound to the B-helix. The structure presented here also provides a context for a number of disease-causing mutations and for further dissection of the mechanisms by which CaM controls Kv7 function.

Introduction

Pore-forming subunits of the Kv7.x (KCNQx) potassium channel family (Kv7.1–Kv7.5) (KCNQ1-KCNQ5)[1–3] form the classically studied M current in neurons (Kv7.2–Kv7.5)[4–6] and I_{KS} current (Kv7.1) in heart, vestibular, and auditory cells.[2,7–9] Kv7 channels open at subthreshold membrane potentials, do not inactivate, and, therefore, provide a strong brake on membrane excitation.[4,10] Consequently, a variety of signaling pathways tune electrical excitability by regulating Kv7 function.[3,4,6] Commensurate with their pivotal role in controlling excitation, Kv7 channels are targets for the development of modulators to treat diseases involving neuronal hyperexcitability such as epilepsy and neuropathic pain.[11–14] Further, mutations in Kv7 channels have been linked to various human diseases, including cardiac arrhythmias, deafness, and epilepsy.[2,14,15]

Kv7 channels have the canonical six-transmembrane architecture found throughout the voltage-gated ion channel family[16] (Fig. 1a). The Kv7 cytoplasmic C-terminal tail (~300–400 residues) comprises approximately half of the total residues of the pore-forming subunit and is composed of four conserved elements known as segments A–D (Fig. 1b; Supplementary Fig. S1).[17,18] This region forms

an important, multifunctional entity that is central to channel assembly, gating, regulation, and the formation of complexes with regulatory factors[17] including calmodulin (CaM).[19–23] Although Kv7 function has been characterized extensively,[4,6,10,14] structural knowledge for this channel class is limited to a portion of the cytoplasmic C-terminal tail, called the D-helix or A domain tail,[18,24,25] which is important for subunit specific assembly. Strikingly, over 60% of the known Kv7 disease mutations occur in the cytoplasmic C-terminal tail where their direct functional consequences are not obvious.[18,26–28] Thus, defining the structure that underlies this hub of Kv7 regulation remains a key objective both for understanding the basic mechanisms by which Kv7 channels are regulated and assembled, and for understanding how disease mutations cause channel dysfunction.

One of the key Kv7 modulation pathways involves interaction between the calcium sensor CaM[19,29,30] and the Kv7 C-terminal cytoplasmic domain.[29] CaM affects the function of all Kv7 subtypes[19–21,29,31,32] by binding to distinct regions within the cytoplasmic C-terminal tail.[19,22,23] Two of these, the A and B segments, have sequence features that have been proposed as CaM binding motifs, an IQ motif in the A segment and two adjacent 1–5–10 motifs in the B segment.[23] Studies of the calcium dependency of the CaM interaction with Kv7.1[18,20,21] and Kv7.2, Kv7.3, and Kv7.4[33] C-terminal tails indicate that both forms of CaM, apo-CaM and Ca^{2+}/CaM, bind to the channel. However, the details of the precise interactions and calcium dependencies remain controversial[17,22,34] and exactly how CaM binds to the channel and how CaM-mediated calcium signals affect channel activity remain unclear.

Here, in an effort to unravel the structural details of the CaM–Kv7 association, we examined the interactions of CaM with the Kv7.4 C-terminal domain. Kv7.4 is a neuronal channel that has been shown to be important for mechanosensation in cochlear outer hair cells[35,36] and touch-sensitive dorsal root ganglia neurons[37] and carries mutations causing autosomal dominant hearing loss known as nonsyndromic sensorineural deafness type 2 (DNFA2).[36] Systematic delineation of the Ca^{2+}/CaM interaction site shows that that the B segment alone constitutes a minimal binding module for Ca^{2+}/CaM. Determination of the crystal structure of the Ca^{2+}/CaM:Kv7.4 B-helix complex at 2.60 Å resolution revealed that Ca^{2+}/CaM binds the B-helix in an antiparallel orientation that uses a novel variation of the 1–14 Ca^{2+}/CaM binding motif. This structure together with our biochemical studies suggests that there is a conformational switch between the apo-CaM and Ca^{2+}/CaM states that involves a change in binding mode from a cross-bridged form using the A and B segments to an antiparallel binding interaction focused on the B-helix.

Results

CaM binds to the Kv7.4 C-terminal tail independently of calcium

To investigate the interaction of CaM with the Kv7.4 C-terminal tail, we co-expressed CaM and a construct bearing the Kv7.4 cytoplasmic C-terminus elements A–D (residues 319–645) fused C-terminal to a His_6-maltose binding protein (MBP)-tobacco etch virus (TEV) protease tag, HMT (termed 'HMT-Q4AD') in *Escherichia coli* and purified the complex under two conditions: high calcium (1 mM $CaCl_2$) and low calcium [1 mM ethylene glycol tetraacetic acid (EGTA)]. Consistent with previous results for the purified Kv7.1 C-terminal tail[18] and with pull-down experiments reported for various glutathione *S*-transferase (GST) fusions of Kv7.2, Kv7.3, and Kv7.4 C-terminal tails,[33] we found by size-exclusion chromatography (SEC) measurements that the purified CaM:Q4AD complexes remained associated independent of the presence of calcium (Fig. 1c).

In the SEC experiments, the purified complexes elute much earlier than what would be predicted for a globular protein of the same size (apparent molecular mass ~380 kDa *versus* the expected molecular mass for a 4:4 complex of 211 kDa). Considering that the apparent molecular mass from SEC relies on the hydrodynamic radius and is, thus, directly affected by the shape of the protein in question,[38] we set out to assess the oligomerization state of the complex more accurately by equilibrium sedimentation experiments, which provide shape-independent mass information.[39,40] Under low-calcium conditions [1 mM ethylenediaminetetraacetic acid (EDTA)], we observed a mass distribution that could be fit by a single-species model and that revealed an apparent molecular mass of 208 ± 17 kDa (Fig. 1d), a value having excellent agreement with the expected molecular mass of a 4:4 CaM:Q4AD complex (221 kDa). This behavior was maintained over a range of starting concentrations (3–40 μM). The 4:4 nature of this complex and the similarity of the SEC behavior between the 1 mM EDTA and 1 mM Ca^{2+} conditions suggest that both the apo- and calcium-bound forms of the CaM:Q4AD complex have a 4:4 stoichiometry.

Identification of Ca^{2+}–CaM and apo-CaM binding sites on the Kv7 C-terminal tail

Previous studies indicated that the Kv7 C-terminal tail A and B segments are candidate CaM binding elements[6,18,20–23,33]; however, opposing observations about the specific role of these domains in the interaction have prevented the proposal of a consensus model. In order to address the contribution of each of the segments to CaM binding within

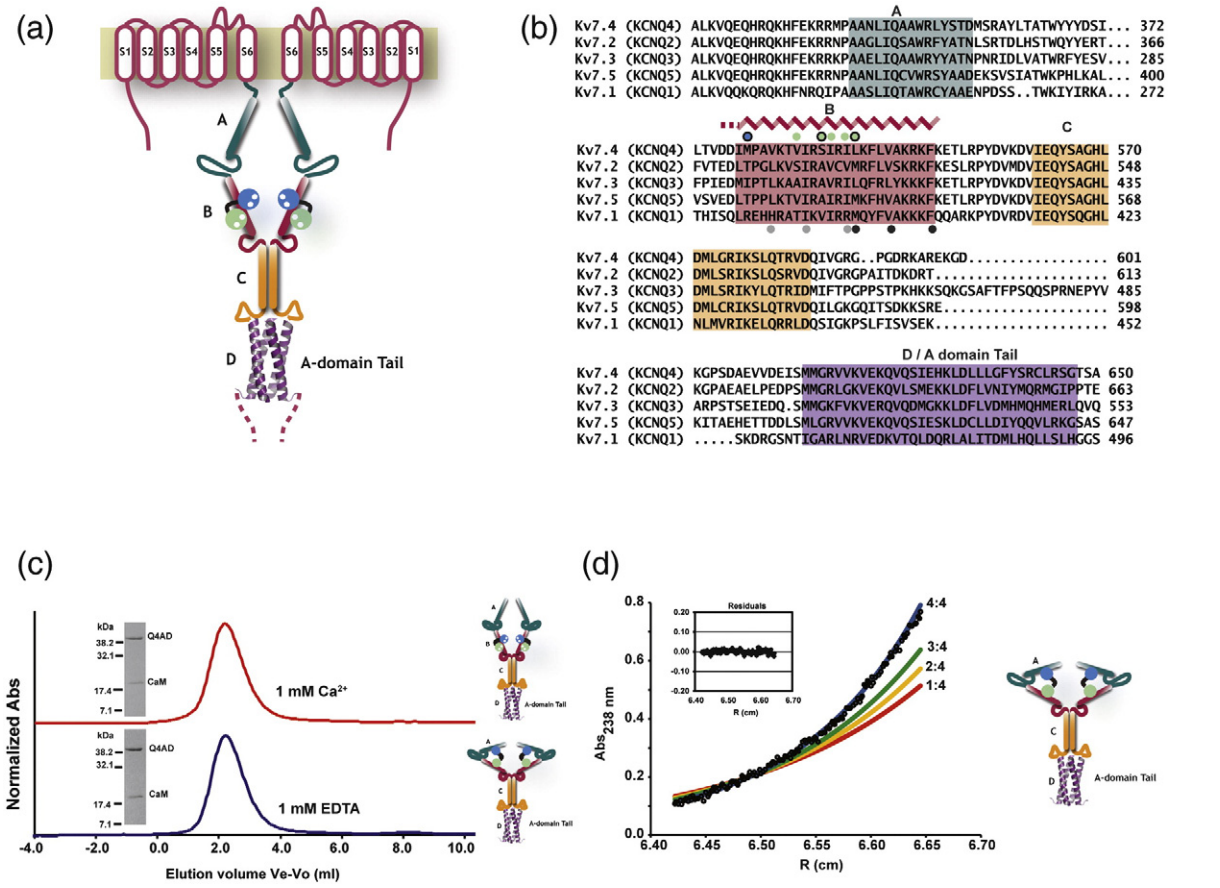

Fig. 1. Kv7 C-terminal tail and interactions with CaM. (a) Kv7 cartoon diagram. Two of the four transmembrane subunits are shown. Transmembrane segments are labeled S1–S6. The four C-terminal tail segments, A–D, are indicated in dark green, red, orange, and purple, respectively. The D segment/A domain tail is shown in cartoon form using the Kv7.4 D segment/A domain tail structure.[24] Broken lines indicate non-conserved C-terminal end. (b) Sequence comparisons of Kv7 tail A, B, C, and D segments. Colors are as in (a). Secondary structure of the B segment is indicated. Blue and green circles indicate Ca^{2+}/N-lobe and Ca^{2+}/C-lobe anchors, respectively. Black open circles indicate the 1–10–14 motif. Gray and black filled circles under the B segments indicate the two suggested 1–5–10 motifs from Yus-Najera *et al.*[23] (c) Superdex200 chromatography of the CaM:Q4AD complexes in the presence (top) and absence (bottom) of calcium. Inset shows peak fraction components. Cartoon represents the state of the investigated complex. (d) Exemplar equilibrium sedimentation data from 238 nm for the 20-μM apo-CaM:Q4AD complex at 7000 rpm. Inset shows residuals from a single-species fit. Blue, green, yellow, and red curves show the expected distributions for 4:4, 3:4, 2:4, and 1:4 CaM:Q4AD complexes, respectively. Cartoon represents the state of the investigated complex. CaM binding orientations in all cartoons are for illustrative purposes only.

the Kv7.4 (KCNQ4) C-terminal tail, we co-expressed CaM with Kv7.4 (KCNQ4) constructs bearing helices B–D (residues 522–645, denoted as 'Q4BD') or C–D (residues 546–645, denoted 'Q4CD') to compare their CaM binding behaviors with the Q4AD construct. Pull-down experiments of the HMT-Q4BD fusion co-expressed with CaM revealed an obvious difference from the Q4AD construct. Although capture of HMT-Q4BD in the presence of 1 mM $CaCl_2$ brought down CaM (Fig. 2a), similar experiments in the presence of 1 mM EDTA failed to pull down CaM even though sufficient amounts had been co-expressed with the HMT-Q4BD fusion (Fig. 2b). Experiments with the HMT-Q4CD construct, which lacks both potential CaM binding elements, showed an absence of interaction with CaM in either the presence or the absence of calcium (Fig. 2c). These data indicate that the B segment is indispensable for the interaction and agree with similar results obtained for a previously reported GST-fusion construct of a similar portion of Kv7.2.[23] Thus, together with the experiments on the Q4AD construct, our data support the notion that the B segment has a prominent role in Ca^{2+}/CaM binding (Fig. 2a and c), whereas the A element appears essential for apo-CaM binding (Figs. 1c and d and 2b), and are in agreement with prior studies of these elements.[19,23]

We were able to purify the Ca^{2+}/CaM:Q4BD complex and analyze its properties by SEC. These experiments showed that in the presence of calcium,

the two components associated in an assembly that was at least as large as a 4:4 complex (Fig. 2d). In contrast, addition of EDTA to the purified Ca^{2+}/CaM:Q4BD complex just prior to SEC resulted in a single peak that was much smaller than the complex and that contained only CaM (Fig. 2d). Under these conditions, the Q4BD portion of the sample precipitated once CaM was disengaged, explaining the absence of the Q4BD component. This behavior is decidedly different from the Q4AD construct in which CaM remained associated in both Ca^{2+}/CaM and apo-CaM states (Fig. 1c) and is consistent with the inability of the HMT-Q4BD fusion to pull down apo-CaM (Fig. 2b). Assessment of the oligomerization state of the Ca^{2+}/CaM:Q4BD complex by equilibrium sedimentation experiments using a range of starting concentrations (10–40 μM) revealed a molecular mass of 124 ± 4 kDa, indicating a 4:4 Ca^{2+}/CaM:Q4BD stoichiometry (expected 125 kDa) (Fig. 2e). This stoichiometry matches that of the Ca^{2+}/CaM:Q4AD complex and confirms that helix A is dispensable for tetramerization of the C-terminal tail. Pull-down experiments using similar BD constructs from the other Kv7 isoforms demonstrate that all are capable of interacting with Ca^{2+}/CaM (Fig. 2f) and indicate that the Ca^{2+}/CaM:Kv7 B segment interaction is common, is calcium dependent in all Kv7 subtypes, and is shared by the entire Kv7 family. SEC of these constructs shows that similar to Q4BD, both Ca^{2+}/CaM:Q2BD and Ca^{2+}/CaM:Q5BD complexes produce clean, well-behaved, tetrameric material (Supplementary Fig. S2).

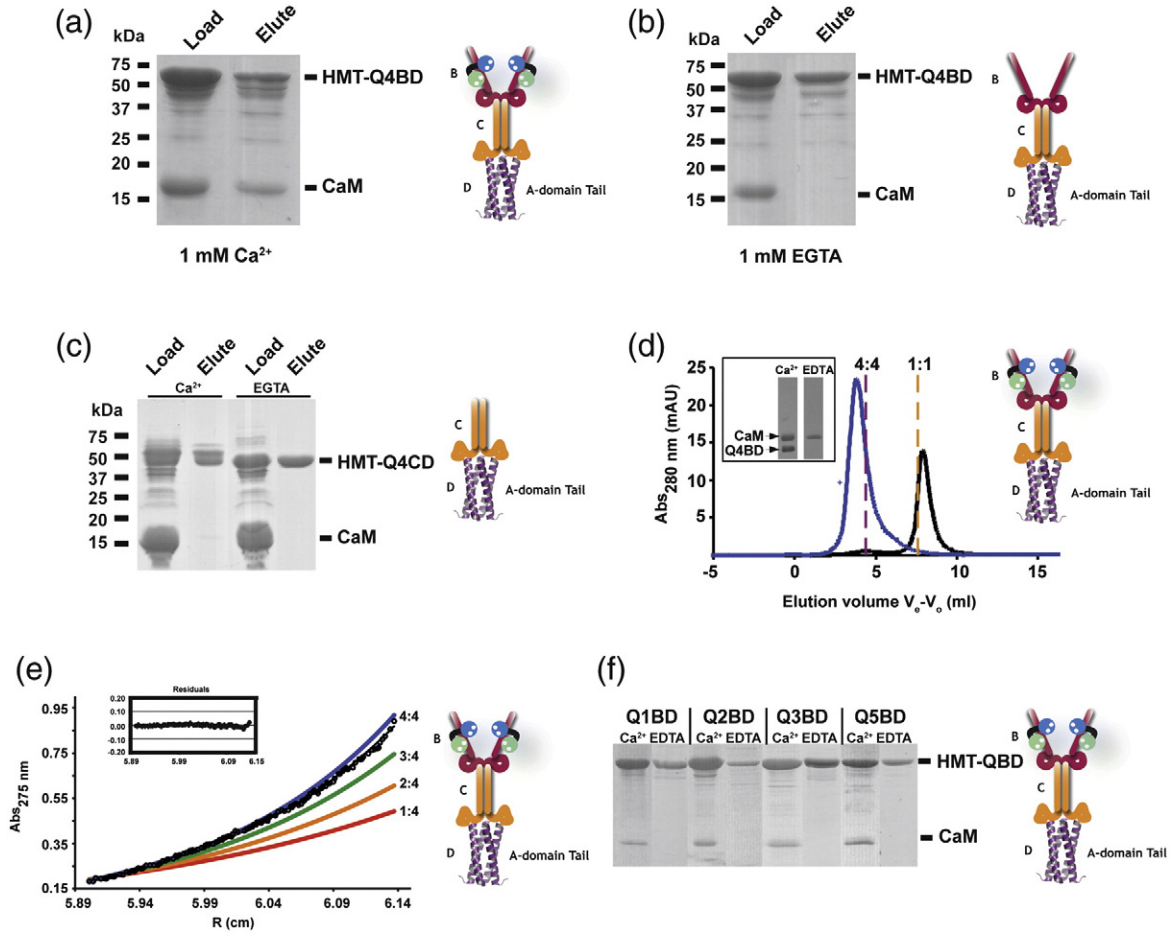

Fig. 2. Kv7.4 B–D interactions with CaM. (a) SDS-PAGE analysis of a pull-down of Ca^{2+}/CaM with Kv7.4 B–D (HMT-Q4BD). (b) SDS-PAGE analysis of pull down of apo-CaM and Kv7.4 B–D (HMT-Q4BD). (c) SDS-PAGE analysis of a pull down of Ca^{2+}/CaM and apo-CaM with Kv7.4 C-D (HMT-Q4CD). (d) Superdex200 SEC showing the behavior of the CaM:Q4BD complex in the presence of 1 mM $CaCl_2$ (blue) and 1 mM EDTA (black). Inset shows peak fractions. (e) Exemplar equilibrium sedimentation data for the Ca^{2+}/CaM:Q4BD complex. Inset shows residuals. Blue, green, orange, and red curves show expected mass distributions for a 4:4, 3:4, 2:4, and 1:4 Ca^{2+}/CaM:Q4BD complex. (f) Exemplar SDS-PAGE analysis of pull-downs showing the calcium-dependent interaction of CaM with each of the Kv7 isoforms: Kv7.1 (Q1BD), Kv7.2 (Q2BD), Kv7.3 (Q3BD), and Kv7.5 (Q5BD). Cartoons indicate the species investigated in each panel.

Kv7 segment B is necessary and sufficient for Ca^{2+}–CaM binding

To define the Ca^{2+}/CaM binding site better, we examined C-terminal deletions of the C and D regions for their ability to bind Ca^{2+}/CaM. Truncation of either the D segment/A domain tail (Q4BC, 522-593) or both the C segment and D segment/A domain tail (Q4B, 522-557) failed to disrupt Ca^{2+}/CaM binding (Fig. 3a). Further investigation by SEC coupled with multiangle light scattering (SEC-MALS)[41,42] showed that at 35 μM, the Ca^{2+}/CaM:Q4BC (residues 522–593) complex forms a monodisperse complex having a 1:1 stoichiometry (Fig. 3b). This result differs from a previous report that indicated that the Kv7.1 C helix alone is dimeric at concentrations below 100 μM.[18] This discrepancy may be due to the fact that the Kv7.1 C segment is different in sequence from that of Kv7.4 (Fig. 1b) or that the presence of Ca^{2+}/CaM perturbs the ability of the C segment to self-associate. SEC-MALS investigation of the Ca^{2+}/CaM:Q4B (residues 522–557) complex found a monodisperse entity having a 1:1 Ca^{2+}/CaM:Q4B stoichiometry (Fig. 3c). The absence of higher-order complexes provides further evidence that the C and D segments are necessary for oligomerization[18,24,43–45] and shows that Ca^{2+}/CaM binding is independent of the oligomeric state of the channel C-terminal tail. The data further demonstrate that the B segment is both necessary and sufficient for Ca^{2+}/CaM binding.

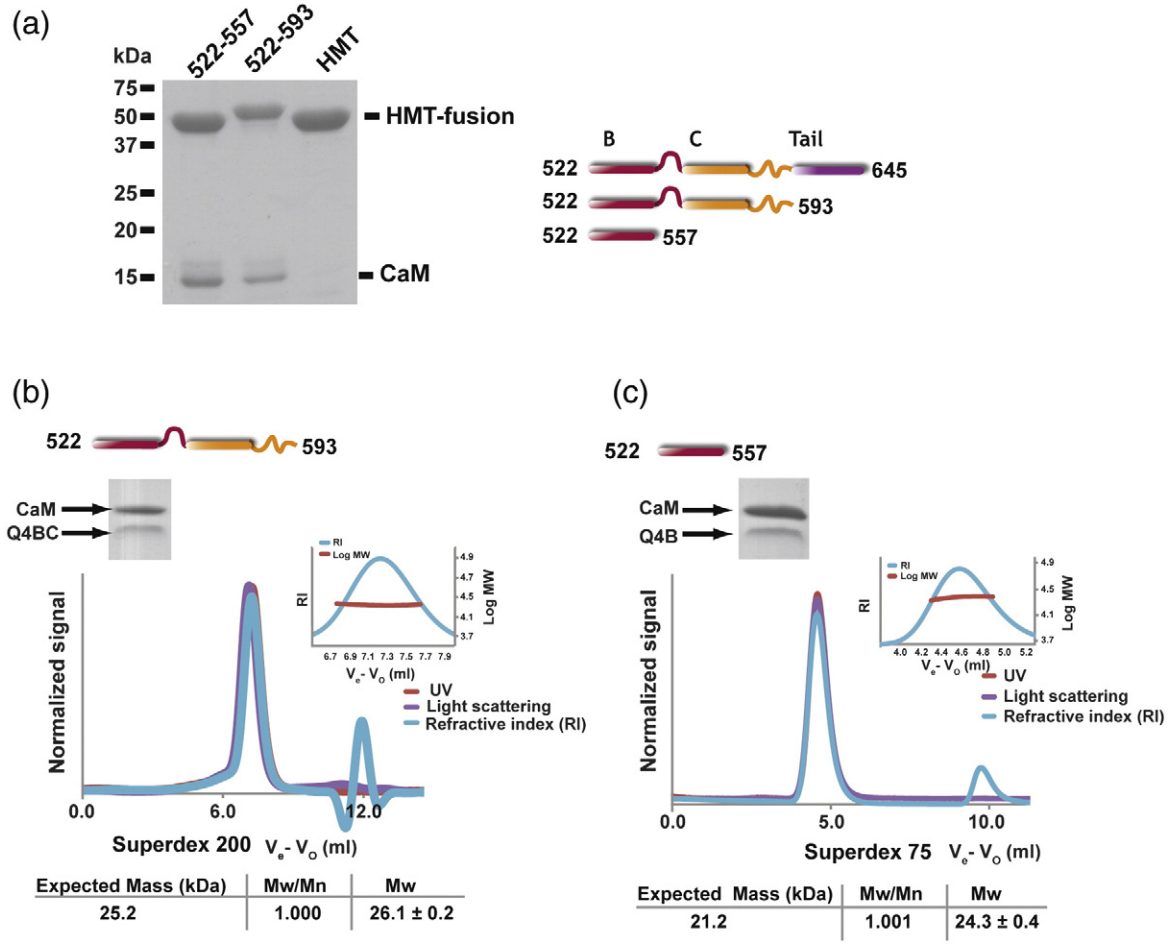

Fig. 3. Characterization of Ca^{2+}/CaM:Kv7.4 B–D interactions. (a) SDS-PAGE analysis of a pull-down of Ca^{2+}/CaM with indicated Kv7.4 BD truncations. Cartoons indicate the domain structure of the various constructs. (b and c) Exemplar SEC-MALS characterization of (b) the Ca^{2+}/CaM:Kv7.4 B–C (Q4BC) complex loaded at a concentration of 35 μM on a Superdex200 column run in a buffer of 200 mM KCl, 1 mM $CaCl_2$, and 10 mM Hepes, pH 7.4, and (c) the Ca^{2+}/CaM:Kv7.4 B (Q4B) complex loaded at a concentration of 80 μM on a Superdex75 column run in a buffer of 200 mM KCl, 1 mM $CaCl_2$, and 10 mM Hepes, pH 7.4. Insets show molecular weight distribution across the main peak and peak fraction SDS-PAGE analysis. MALS-derived parameters and expected molecular masses for a 1:1 Ca^{2+}/CaM:Kv7.4 complex are shown.

Table 1. X-ray data collection and refinement statistics

	Ca^{2+}/CaM:Kv7.4 B-helix complex
Data collection	
Wavelength (Å)	1.006
Resolution (Å)	50–2.60 (2.74–2.60)
Space group	$P6_522$
Cell dimensions	
a, *b*, *c* (Å)	104.01, 104.01, 113.72
α, β, γ (°)	90, 90, 120
R_{sym} (%)	10.3 (96.4)
R_{pim} (%)	2.6 (28.3)
$I/\sigma I$	19.1 (2.8)
Completeness (%)	100 (100)
Redundancy	16.7(12.7)
Refinement	
Number of reflections (work/test)	11,699/562
R_{work}/R_{free}	24.0/26.5
Number of atoms	
Protein	1340
Water	18
Average *B*-factor (Å^2)	27.2
RMSD	
Bond lengths (Å)	0.003
Bond angles (°)	0.778
Ramachandran plot	
Favored region (%)	93.2
Allowed region (%)	6.8

Values in parentheses are those for the highest-resolution shell.

Structure of the Ca^{2+}–CaM/Kv7.4 (KCNQ4) B-helix complex

We were able to grow crystals from hanging drop setups containing the Ca^{2+}/CaM:Q4BC (Kv7.4 residues 522–593) complex. The best of these was a hexagonal crystal form that diffracted X-rays to 2.60 Å resolution (Table 1). Structure determination by molecular replacement using the N-lobe polypeptide from the Ca^{2+}/CaM:smooth muscle myosin light chain kinase (sMLCK) peptide complex[46] showed that the asymmetric unit contained only a single Ca^{2+}/CaM:peptide complex comprising one Ca^{2+}/CaM bound to an α-helix formed by Kv7.4 B segment residues Asp524-Phe549 (Fig. 4a and Supplementary Fig. S3). Subsequent mass spectroscopy analysis of the crystallization mixture revealed that the Q4BC construct had been truncated at residue 551 during the process of crystallization leading to the hexagonal crystal. This deletion essentially removed the entire C segment (cf. Materials and Methods) and explains its absence from the structure.

The structure revealed that Ca^{2+}/CaM wraps around the Kv7.4 B-helix in an antiparallel orientation in which the Ca^{2+}/C-lobe and Ca^{2+}/N-lobe bind to the N-terminal and C-terminal portions of the target helix, respectively. This interaction buries a substantial amount of surface area, 2831 Å^2, of which 1570 Å^2 is hydrophobic. Kv7.4 B-helix residues Met527 and Leu540 form the most distant Ca^{2+}/CaM anchors and comprise a 1-14 motif.[47,48] Hence, we indicate each of the residues in helix B by both the residue number and the indicator number 1 through 14 with respect to this motif (Fig. 4b). This binding motif was first described in Ca^{2+}/CaM complexes with the M13 peptide from sMLCK[46,49] and is regarded as a motif that is specific to Ca^{2+}/CaM binding rather than apo-CaM binding.[47] Prior studies had suggested that the B segment had two possible 1–5–10 Ca^{2+}/CaM binding motifs (Figs. 1b and 4b).[23] Although some of the residues in these putative 1–5–10 motifs interact with Ca^{2+}/CaM, neither of these motifs forms the heart of the Ca^{2+}/CaM:Kv7.4 B-helix interaction. Further, the conserved aromatic residues at the (16) and (23) positions (Kv7.4 Phe542 and Phe549), including the key (10) position of the second putative 1–5–10 motif (Fig. 4b), do not interact with Ca^{2+}/CaM.

Of the two Ca^{2+}–CaM lobes, Ca^{2+}/N-lobe makes more extensive interactions with the B-helix (1764 Å^2 *versus* 1068 Å^2 buried surface, for Ca^{2+}/N-lobe and Ca^{2+}/C-lobe, respectively). The C-terminal anchor of the 1–14 motif, Leu540 (14), resides in a pocket formed by Ca^{2+}/N-lobe residues Phe19, Leu32,

Fig. 4. Ca^{2+}/CaM:Kv7.4 B-helix complex structure. (a) Ca^{2+}/CaM:Kv7.4 B-helix complex. Ca^{2+}/CaM N-lobe and C-lobe are shown in green and blue, respectively. Kv7.4 B-helix is shown in firebrick with side chains shown as sticks. N- and C-terminal ends of the B-helix are labeled. Axial view is from the B-helix C-terminal end. Positions of the 1–14 anchors are indicated. (b) Sequence comparison of Kv7 B-peptide segments. Residues shaded in blue, green, and purple indicate Kv7.4 positions contacted by Ca^{2+}/C-lobe, Ca^{2+}/N-lobe, and both lobes, respectively. Colors on other Kv7 sequences indicate conserved contact residues. B-helix secondary structure is indicated. Blue and green circles indicate Ca^{2+}/N-lobe and Ca^{2+}/C-lobe anchors, respectively. Black open circles indicate the 1–10–14 motif. Gray and black filled circles under the alignment indicate the two suggested B segment 1–5–10 motifs from Yus-Najera *et al.*[23] Orange squares indicate positions of disease mutants in Kv7.1 and Kv7.2 B segments. (c and d) Details of (c) Ca^{2+}/C-lobe:Kv7.4 B-helix and (d) Ca^{2+}/N-lobe:Kv7.4 B-helix interactions. Ca^{2+}/C-lobe and Ca^{2+}/N-lobe are shown as semitransparent surfaces and sticks. Hydrophobic, basic, acidic, and polar side chains from CaM are colored yellow, blue, red, and green, respectively. Kv7.4 B-helix is shown as sticks and colored firebrick with nitrogen and oxygen atoms colored blue and red, respectively. Kv7.4 anchor side chains are colored pink. In both panels, key residues of Ca^{2+}/CaM are labeled using the single-letter code. Kv7.4 B-helix residues are labeled using the three-letter code followed by the position number within the 1–14 motif, indicated in parenthesis. (e) Locations of Kv7.1 and Kv7.2 disease mutants, colored orange and indicated using the three-letter code, mapped on the Ca^{2+}/CaM:Kv7.4 B-helix structure. Ca^{2+}/N-lobe is colored green with nitrogen and oxygen atoms colored blue and red, respectively. CaM residues are indicated using the single-letter code. White broken lines indicate the electrostatic interactions for Arg547–Glu54 (2.1 and 2.7 Å) and Lys548–Asp50 (4.2 Å).

Met51, Phe68, and Met71 (Fig. 4c). Ca^{2+}/N-lobe also has extensive contacts with the B-helix residues Val533 (7), Ser536 (10), Ile537 (11), Ile539 (13), and Leu540 (14) (Supplementary Fig. S4). Of these, Val533 (7), Ser536 (10), and Leu540 (14) are the most buried. Ca^{2+}/C-lobe interactions are centered on Kv7.4 Met527 (1), which is buried in a methionine-rich pocket formed from CaM residues Phe92, Leu105, Met109, Met124, Met144, and Met145 (Fig. 4d and Supplementary Fig. S4). Additionally, a number of B-helix residues form salt bridges and hydrogen bond interactions with Ca^{2+}/N-lobe (Lys 531, Arg547, and Lys548), Ca^{2+}/C-lobe (Arg538), or both (Arg535).

In good agreement with the commonality of the Ca^{2+}/CaM:B segment interaction (Fig. 2), the size and hydrophobicity of the majority of key Ca^{2+}/N-

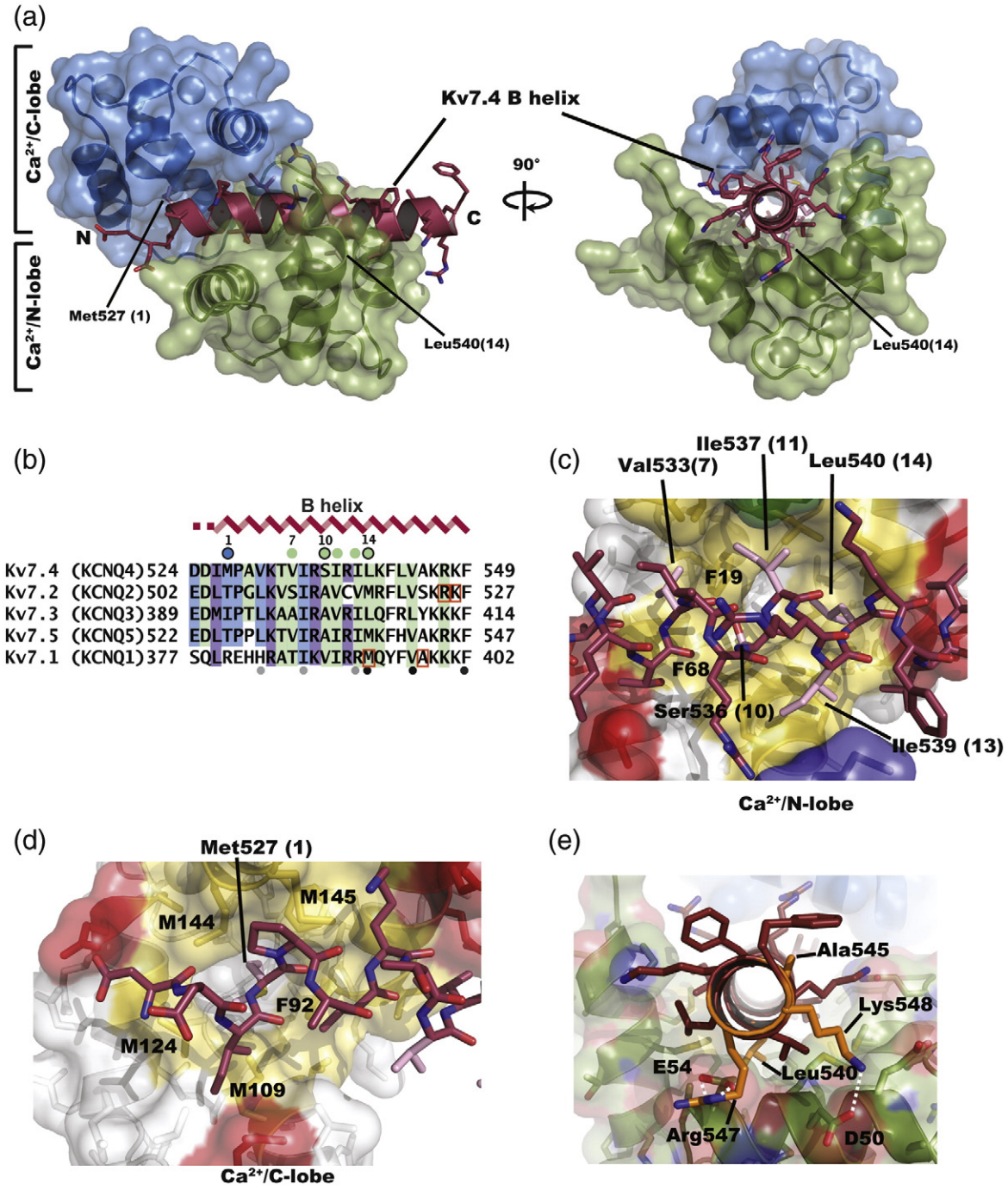

Fig. 4 (*legend on previous page*)

lobe contact residues (positions 7, 10, 11, and 14) are well conserved among the Kv7 family (Fig. 4b). One Ca^{2+}/N-lobe contact, position (13) (Kv7.4 Ile539), is an arginine in Kv7.1, but as this residue is not completely buried, it seems possible that both the hydrophobic and charged natures of the arginine could be accommodated by the binding mode seen for Kv7.4 (Fig. 4d). Besides the 1–14 anchors, the other highly buried position is Ser536 (10). The γ-hydroxyl of this residue is buried in a hydrophobic environment (Supplementary Fig. S5) in which the nearest polar contact is to the Val533 backbone carbonyl (2.7 Å). Notably, this position is conserved as a small residue among the Kv7s (Fig. 4b). From this perspective, the Kv7 B-helix Ca^{2+}/CaM binding motif could be considered a 1–10–14 variation on the 1–14 motif.

The observed interaction network is in line with reported effects of aspartate mutants in the Kv7.2 B segment[23] in which a Ser→Asp change at position (7) (Kv7.4 V533) interfered with Ca^{2+}/CaM binding,[23,34] whereas an Ala→Asp change at position (19) (Kv7.4 Ala545), which makes no contacts, showed no effect. In contrast to the high conservation of Ca^{2+}/N-lobe anchor sites, Ca^{2+}/C-lobe contact sites (Fig. 4b) are more varied. In particular, the identity of the (1) position is not well conserved and is a positively charged residue in Kv7.1. Other Ca^{2+}/C-lobe contact positions, Asp524, Pro528 (2), and Val529 (4), are well conserved among the neuronal channels, Kv7.2–Kv7.5, but all have changes in charge in Kv7.1. It is possible that these differences underlie the apparent difference in the CaM response of Kv7.1 *versus* the other Kv7s.[19–21]

Location of B-helix disease mutants and regulatory sites

Kv7 channels bear a large number of human mutations that cause cardiovascular and hearing disorders and epilepsies.[15,26,50] The conservation of the key anchoring residues in the B-helix (Fig. 4b) allows the identification of the positions of a number of known disease mutants from other Kv7 channels within the context of the Ca^{2+}/CaM:Kv7.4 B-helix complex structure. Of the four reported B-helix disease mutants, three occur at positions that contact the Ca^{2+}/N-lobe. The Kv7.1 mutant M520R[51] corresponds to anchor position (14) in the 1–14 motif, Leu540 in Kv7.4 (Fig. 4b and d). In accordance with the buried nature of this position, the M520R change has been reported to disrupt both channel function and CaM binding.[51] Two Kv7.2 mutations, R533Q[26,52] and K562N,[53] correspond to Kv7.4 positions Arg547 and Lys548 (Fig. 4b) that make electrostatic interactions with Ca^{2+}/N-lobe residues Glu54 and Asp50, respectively (Fig. 4e), and would disrupt these electrostatic contacts. The fourth reported mutant, Kv7.1 A525T,[54] corresponds to Kv7.4 Ala545, a residue having no contacts with Ca^{2+}/CaM (Supplementary Fig. S4). Because the B segment is involved in both apo-CaM and Ca^{2+}/CaM binding, it is not possible from the structure alone to know whether the disease mutations act by affecting apo-CaM binding, Ca^{2+}/CaM binding, or both. Nevertheless, the structure provides an important context for further studies addressing this question.

In addition to the effects that B-helix mutations have on function, a pair of studies by Shapiro *et al.* has shown that *N*-ethylmaleimide (NEM) treatment, a channel opener that acts by covalent modification of a cysteine residue that is part of the B segment, blunts the effects of Ca^{2+}/CaM suppression of Kv7.2, Kv7.4, and Kv7.5 currents.[29,55] This effect is competitive with CaM action, a result that has suggested overlapping sites of action.[29] Although the cysteine responsible for this NEM effect was not present in the crystallized construct, it is just five residues away from the N-terminal end of the B-helix

Fig. 5. Comparison of the Ca^{2+}/CaM:Kv7.4 B-helix complex with other 1–14 Ca^{2+}/CaM complexes. (a) Superposition of the Ca^{2+}/CaM:Kv7.4 B-helix complex with the M13 peptide of smooth muscle myosin light chain kinase (cyan), sMLCK (1CDL).[46] The sMLCK complex is shown in light blue and cyan. Calcium ions are indicated as white (Kv7.4 complex) and gray (sMLCK) spheres. Residues from sMLCK are labeled in italics. Residues from the Kv7.4 complex are labeled in boldface. (b–e) Comparisons of the Ca^{2+}/CaM:Kv7.4 B-helix complex with other 1–14 Ca^{2+}/CaM complexes. In each case, the (1) position or (14) position residue is shown in sticks and labeled. Residues in italics and surfaces come from the sMLCK, eNOS, and DAPK structures. Kv7.4 residues are labeled in boldface. Ca^{2+}/CaM residues are indicated using the single-letter code. In all panels, the Ca^{2+}/CaM from the Kv7.4 complex is shown in marine and the Met527 side chain is shown in firebrick. Nitrogen, oxygen, and sulfur atoms are colored blue, red, and yellow, respectively. (b) View of the Ca^{2+}/C-lobe interactions surrounding the (1) position of the 1–14 motif for the Ca^{2+}/CaM:sMLCK complex. Ca^{2+}/CaM:sMLCK is in light blue. sMLCK Trp800 is in cyan. sMLCK Ca^{2+}/CaM C-lobe RMSDs are 0.568 and 1.375 for C^{α} and all atoms, respectively. (c) Comparison of the (14) position binding pocket for Ca^{2+}/CaM:sMLCK and Ca^{2+}/CaM:Kv7.4 B-helix. Colors are as in (b). sMLCK Leu813 is in cyan. Ca^{2+}/CaM N-lobe RMSDs are 0.914 and 1.636 for C^{α} and all atoms, respectively. (d) Comparison of the (1) position binding pocket for the Ca^{2+}/CaM:eNOS complex (1N1W)[57] and Ca^{2+}/CaM:Kv7.4 B-helix. The Ca^{2+}/CaM:eNOS complex is shown in orange. eNOS Phe465 is in olive. Ca^{2+}/CaM C-lobe RMSDs are 1.085 and 1.520 for C^{α} and all atoms, respectively. (e) Comparison of the position 1 binding pocket for the Ca^{2+}/CaM:DAPK (1YR5) complex and Ca^{2+}/CaM:Kv7.4 B-helix.[58] Ca^{2+}/CaM:DAPK is shown in white. DAPK Trp305 is in tan. Ca^{2+}/CaM C-lobe RMSDs are 0.903 and 1.648 for C^{α} and all atoms, respectively. (f) Sequence comparison of target peptides from the Kv7.4, sMLCK, eNOS, and DAPK structures. Blue and green circles indicate Ca^{2+}/N-lobe and Ca^{2+}/C-lobe anchors. Black open circles indicate the 1–10–14 motif.

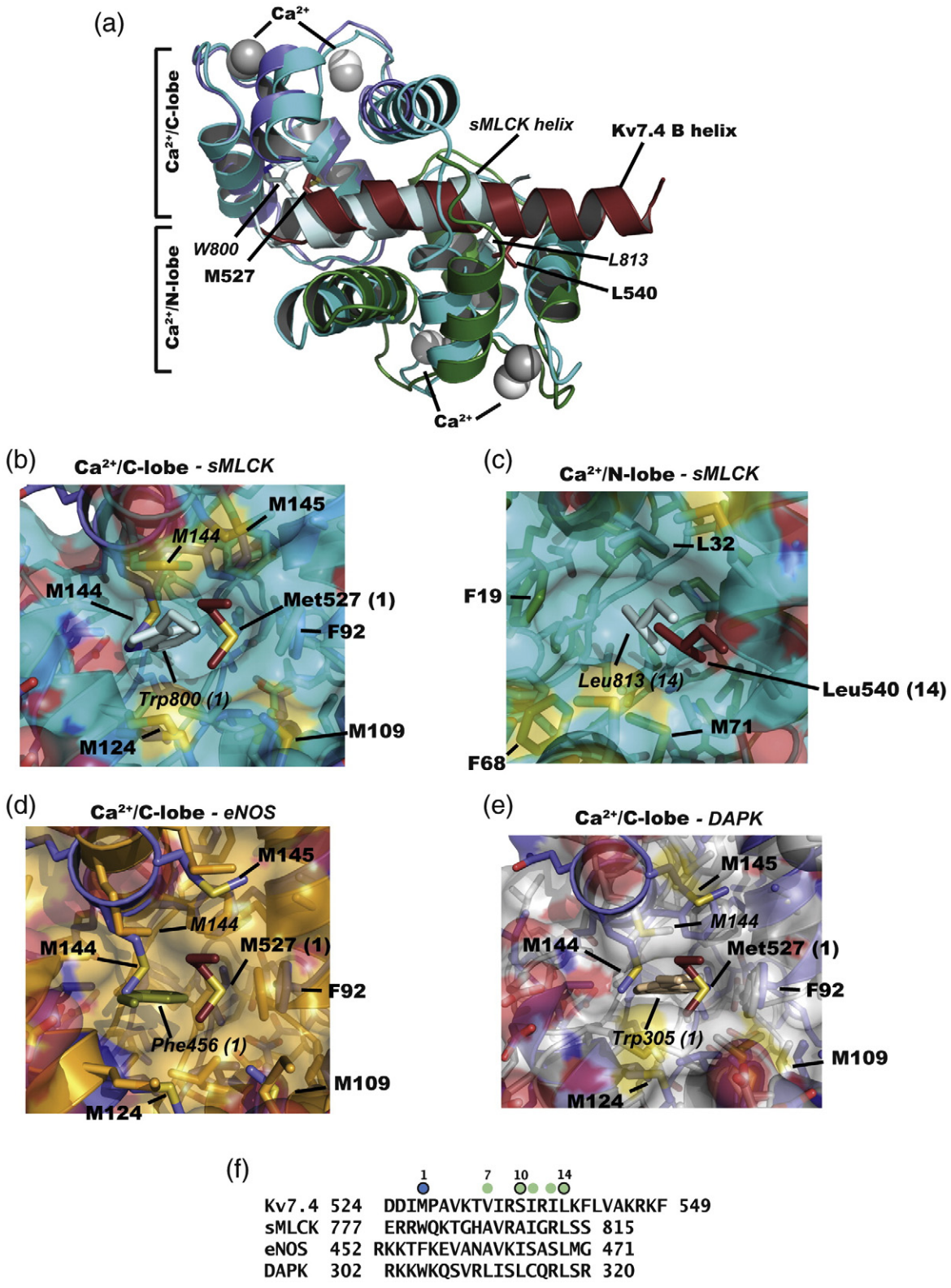

Fig. 5 (*legend on previous page*)

(Supplementary Fig. S1). Examination of the structure suggests that given the covalent constraints of the polypeptide backbone, this cysteine should be near enough to contact Ca^{2+}/C-lobe and thus account for the interfering effects of NEM on Kv7 function, CaM binding, and the antagonistic relationship between NEM and CaM.[29] Importantly, both Kv7.1 and Kv7.3, which are NEM insensitive,[56] lack a cysteine at the equivalent position[29] (Supplementary Fig. S1).

Comparison of the Ca^{2+}/CaM:Kv7.4 B-helix structure with canonical Ca^{2+}/CaM:1–14 motif structures

The original analysis of the B segment sequence predicted two 1–5–10 motifs (Fig. 4b),[23] neither of which are used in Ca^{2+}/CaM binding, but did not predict the 1–14 motif observed in the Ca^{2+}/CaM:Kv7.4 B-helix structure (Fig. 4a–d). Hence, we were interested to compare the Ca^{2+}/CaM:Kv7.4 B-helix complex to other Ca^{2+}/CaM:1–14 motif complexes to examine points of commonality and differences. Structure comparison with the Ca^{2+}/CaM:sMLCK peptide structure[46] that originally defined the 1–14 motif showed that faithful to the 1–14 motif, the 14 residue spacing of anchor positions, Trp800 (1) and Leu813 (14) for sMLCK and Met527 (1) and Leu540 (14) for the Kv7.4 B-helix, places the Kv7.4 B-helix anchor positions on opposite faces of the α-helix where they can independently engage the two Ca^{2+}/CaM lobes (Fig. 5a). Notably, comparison of the structures reveals that the Kv7.4 B-helix is longer than the sMLCK helix by approximately three turns and makes more Ca^{2+}/N-lobe contacts. Although the overall C^{α} RMSD for both complexes is 2.59 $Å^2$, indicating some global differences that are due in part to the longer target peptide in the Kv7.4 structure, the conformations of the individual Ca^{2+}/CaM lobes are very similar and have C^{α} RMSDs of 0.91 $Å^2$ and 0.57 $Å^2$ for Ca^{2+}/C-lobe and Ca^{2+}/N-lobe, respectively.

Examination of the local environments of the (1) and (14) anchor positions shows that these residues bind pockets formed from the same Ca^{2+}/CaM lobe residues in both the Kv7.4 and sMLCK structures (Fig. 5b and c). The (1) position, Kv7.4 Met527 and sMLCK Trp800, binds to a pocket formed by Ca^{2+}/C-lobe residues Phe92, Met109, Met124, Met144, and Met145 (Fig. 5b). Notably, there is a rather large difference in the way the (1) position residues occupy the Ca^{2+}/C-lobe pocket. Kv7.4 Met527 is much closer to the wall of the pocket made by CaM residue Phe92, whereas sMLCK Trp800 is more central to the pocket. In concert with the changes seen at the Kv7.4 (1) position anchor, CaM residue Met144 adopts a side-chain rotamer that reduces the pocket size relative to the sMLCK complex. This conformational difference is consistent with the change from a large aromatic anchor, Trp800, to a smaller and less constrained hydrophobic residue, Met527 (Fig. 5b). In contrast, the Kv7.4 and sMLCK (14) position anchors of residues Leu813 and Leu540, respectively, occupy a pocket formed by Ca^{2+}/N-lobe residues Phe68, Met71, Leu32, and Phe19 that has similar features in both structures (Fig. 5c).

To see whether the differences in the 1–14 interaction were particular to the comparison with the classic sMLCK interaction or more specifically related to the Kv7.4 complex, we conducted a survey to identify all current known 1–14 complexes. This search identified 11 Ca^{2+}/CaM:1–14 complexes (Supplementary Table 1). The difference in the placement of the (1) position residue and the shape of the pocket around Ca^{2+}/CaM Met144 remain vis-à-vis the Kv7.4 B-helix interactions with respect to all complexes from this set. These differences are exemplified by the Ca^{2+}/CaM:endothelial nitrogen oxide synthase (eNOS) peptide complex [Protein Data Bank (PDB) code: 1NIW][57] (Fig. 5d) and a Ca^{2+}/CaM complex with an autoregulatory domain peptide from the death-associated protein kinase DAPK (PDB code: 1YR5)[58] (Fig. 5e). The structure having a non-aromatic at position (1), Leu in human inducible nitric oxide synthase (iNOS)[PDB code:3HR4],[59] has a Ca^{2+}/C-lobe pocket similar to the other structures but has a very different pitch of the target helix, which deviates from the other complexes by ~30° and results in a placement of the (1) position residue midway between the aromatic position from sMLCK Trp800 and the position occupied by Kv7.4 Met 527. These observations provide additional support for the idea that the distinctive structural features we note in the Kv7.4 complex relative to other 1–14 complexes result from accommodation of a non-aromatic at the (1) position. The presence of the non-aromatic (1) position residue further stands out as aromatic residues occupy the Ca^{2+}/C-lobe pocket in a large number of Ca^{2+}/CaM complexes.[60] In light of this analysis, and considering that the canonical pattern of residues at the 1 and 14 positions is defined by the presence of one of five hydrophobic residues (Phe/Ile/Leu/Val/Trp) at the 1 and 14 positions,[47] it is clear how the 1–14 pattern could be missed. Notably, none of the Kv7s have a canonical residue at the (1) position (Fig. 4b). Undoubtedly, the well-known adaptability of CaM stands behind this observation and underscores the importance of experimental determination of Ca^{2+}/CaM:peptide structures.

Discussion

The ability to open at membrane potentials that are below those required to initiate action potentials together with a lack of inactivation sets Kv7 channels

in a key position to control electrical excitability in both the heart and nervous system.[4,10] Hence, they are subject to a wide range of regulatory pathways;[3,4,6] have been identified as molecules in which misfunction underlies a variety of disorders in the cardiovascular, hearing, vestibular, and nervous systems;[2,14,15] and are attractive targets for a range of hyperexcitability disorders.[11–14] CaM is a key regulator and affects the function of all Kv7 subtypes through interactions made in both its apo- and calcium-bound forms with the C-terminal tail of the channel.[19–21,29,31,32] Although the importance of CaM for Kv7 modulation has been long appreciated, the details of the interactions of CaM with the channel have remained unclear. Our data provide new biochemical and structural information that directly bear on the question of how CaM interacts with the channel in both apo- and calcium-bound forms.

In agreement with previous evidence,[22,23] we found that apo-CaM binding to the Kv7.4 C-terminal tail strictly requires the presence of both the A and B segments (Figs. 1c and d and 2b). Importantly, we show directly by sedimentation equilibrium studies that the interaction between apo-CaM and the Kv7.4 construct spanning the A–D segments (Q4AD) has a stoichiometry of 4:4 (Fig. 1d), a result that is consistent with prior sedimentation equilibrium[18] and chemical cross-linking studies of a similar Kv7.1 C-terminal domain construct.[20] This situation is striking as more than 100 amino acids separate the A and B segments. Such a large insertion precludes a contiguous binding site as first noted by Yus-Najera *et al.*[23] and suggests that apo-CaM may use a bidentate binding mode to interact with these non-contiguous sites. There are a number of precedents that indicate that CaM is able to make this sort of bridged interaction,[61–63] most notably, those from the interaction of CaM and the intracellular domains of small-conductance (SK) potassium channel intracellular domains.[62,63] Although there are no structural examples of a complete bridged structure formed by apo-CaM, such an interaction would be very much in line with the ability of the independent apo-CaM lobes to engage targets.[61,64–66] It should be noted that our data do not distinguish whether the apo-CaM interaction with the A and B segments is intrasubunit or intersubunit. Prior studies of the oligomerization behavior of a Kv7.1 construct spanning just the A–B segments indicated the presence of a 1:1 complex in both the presence and absence of calcium and suggest that the apo-CaM cross bridge is intrasubunit.[18] Nevertheless, in the context of the full-length channel, both configurations are reasonable possibilities given the proximity of the intracellular domains, which are constrained by both the interactions of the pore-forming regions in the membrane at one end and those from the D segment/A domain tail[18,24] at the other. Thus, based on the available data, we favor the interpretation that the apo-CaM bridging occurs within a single subunit. Nevertheless, further tests in the context of the full-length channel will be required to address this issue definitively.

In contrast to the complex interactions made by apo-CaM, both our structural and biochemical data indicate that Ca^{2+}/CaM requires only the B segment (Figs. 3c and 4). This interaction involves a classic, contiguous Ca^{2+}/CaM binding site formed by a single α-helix (Fig. 4). Ca^{2+}/CaM wraps around the B segment helix in an antiparallel orientation that uses a variation of the well-described 1-14 binding motif[47,48] in which the two most distant anchoring positions are Met527 and Leu540. This binding mode contrasts with the original suggestion that Ca^{2+}/CaM might interact via 1–5–10 motifs found in the B segment[23] (Fig. 4b) and has a pattern of buried and exposed residues that matches the reported effects of aspartate mutants on CaM binding.[23]

Consistent with the observation that constructs bearing the B-helix from all Kv7 isoforms are able to bind Ca^{2+}/CaM (Fig. 2f), the main determinants of this interaction are conserved throughout the Kv7 family (Fig. 4b). One feature that stands out from other 1-14 Ca^{2+}/CaM target structures is that rather than an aromatic residue at the 1 position, the Kv7.4 B-helix has a methionine. This substitution of an aromatic for a long hydrophobic side chain is readily accommodated by a small rearrangement in the Ca^{2+}/C-lobe binding pocket. Interestingly, all Kv7 isoforms have a non-aromatic residue at the (1) position of the 1-14 motif (Fig. 4b).

Functional studies indicate that the neuronal channels Kv7.2, Kv7.4, and Kv7.5 share a common mechanism of calcium-induced current suppression that involves CaM.[19,29] However, this property is not shared by all members of the family, and most notably, the calcium sensitivity of Kv7.1 has been a point of controversy.[17] Some studies have reported CaM involvement in calcium-dependent activation of Kv7.1 channels,[20,21,67] whereas other studies have failed to find this response.[29] Because the modulation of Kv channels is complex,[3,4,6] it is possible that the reported differences are due to the effects of other CaM-dependent pathways, such as the one involved in S-nitrosylation signals.[32,67] Regardless, it is clear that Kv7.1 behaves differently with respect to CaM than the neuronal Kv7s. It is notable that even though Ca^{2+}/CaM binds C-terminal constructs bearing the B-helix regardless of the Kv7 isoform tested (Fig. 2f), there is a substantial divergence in the residues that would form the Ca^{2+}/C-lobe contacts in Kv7.1 (KCNQ1), including a number of charged residues. Such differences may underlie the functional differences between the CaM-dependent responses of Kv7.1 *versus* the neuronal Kv7s. Additionally, there are differences at the (1) position that could play a role in tuning the CaM responses of the neuronal Kv7s in a subunit-specific manner. Our

new structural data should help to guide further investigation of this phenomenon.

Studies of the calcium dependency of CaM interaction with Kv7.2, Kv7.3, and Kv7.4 C-terminal tails indicate that both apo-CaM and Ca^{2+}/CaM bind.[22,23,33] The presence of apo-CaM binding sites in the A[22,23] and B[23] segments of Kv7.2, together with the observations that the A/B region binds apo-CaM better than the individual segments[23] and that Ca^{2+}/CaM favors binding to the B segment in Kv7.2–Kv7.5,[19] matches well with our observations of the interaction seen using purified components. A number of previous proposals have suggested a cross-bridged binding mode for apo-CaM.[22,23] Consideration of our new data together with this prior work leads us to propose an extension of the CaM modulation hypothesis to include a conformational switch between the apo-CaM and Ca^{2+}/CaM states that involves a change from a cross-bridged form in the apo-CaM state to a classic Ca^{2+}/CaM–helix interaction in the calcium-bound form as seen in our crystal structure of the Ca^{2+}–CaM/Kv7.4 B-helix complex (Fig. 6). Because one of the parts of the bidentate binding site, the A segment, is very near the likely end of the pore-lining transmembrane segment S6, it is reasonable to posit that such a conformational change would affect channel function. For example, the interaction of apo-CaM with the A segment may affect S6 in a way that favors channel opening and, in contrast, when CaM switches to the Ca^{2+}–CaM site on the B-helix, loss of the A segment interaction causes the current to be suppressed. This hypothesis would explain one mechanism for calcium-dependent suppression of neuronal Kv7s. As mentioned above, the response of Kv7.1 to calcium is complicated and unlike that of the neuronal Kv7s. Given that the Kv7.1 B-helix binds Ca^{2+}/CaM, even though the Ca^{2+}/C-lobe site is quite different, Kv7.1 may use some variant of this proposal.

The idea that there would be a structural transition between a bidentate apo-CaM clamp to a calcium-bound form in which the Ca^{2+}/CaM interactions are restricted to the B-helix fits well with the observed, antagonistic effects of NEM alkylation at a B-helix cysteine[29,55] and with the data showing that the calcium sensitivity of the N-lobe is crucial.[29] Such a model would also be consistent with the known importance of the C-terminal tail region that spans the A and B segments for modulation of Kv7 channels by phosphatidylinositol 4,5-bisphosphate[68] and S-nitrosylation[32] and suggests that these various inputs can be coupled in a way that makes the A–B region a signal integration domain. In this regard, it is striking that the sequence that links the A and B segments varies among the Kv7 isoforms in comparison to the A, B, C, and D segments (Fig. S1) and is the site of Kv7.4 splice variation that affects function.[69]

Overall, our data are in agreement with the existence of two CaM binding sites on Kv7 channels, one Ca^{2+} independent and one Ca^{2+} dependent that confers Ca^{2+} sensitivity to the channel.[17] The structure of the Ca^{2+}/CaM:Kv7.4 B-helix complex

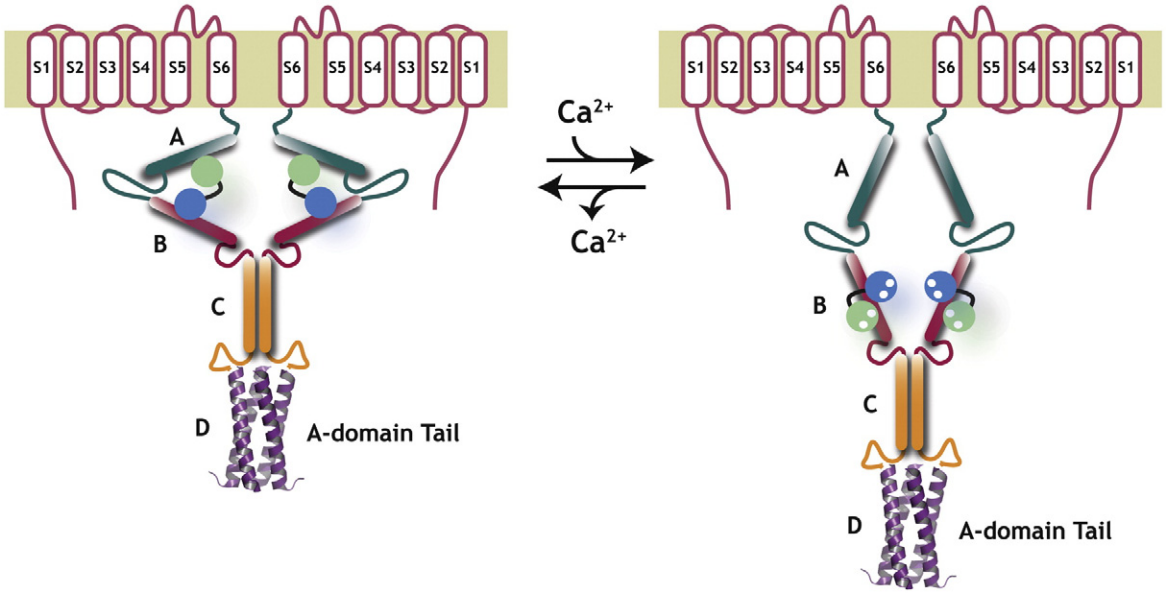

Fig. 6. Model for the calcium-dependent interactions of neuronal Kv7 channels and CaM. Cartoon model depicts the proposed calcium-dependent switch from the cross-bridged apo-CaM binding state (left) to the Ca^{2+}/CaM bound state (right). CaM lobes are indicated as green (C-lobe) and blue (N-lobe). Only two of the four subunits are shown. It should be noted that the exact binding mode for the apo-CaM state is not known. Sequences following the D-helix/A domain tail are omitted from the cartoon for clarity.

shows that a number of Kv7 disease mutations fall at positions that make direct contacts with Ca^{2+}/CaM. However, as the B segment is also involved in apo-CaM binding[22,23] and interactions with CaM may have important effects in channel folding and trafficking,[20,21,70,71] such mutations may interfere with multiple layers of CaM control of the channel. The structure presented here provides a key context for further dissection of the complex effects of Kv7 disease mutants. Finally, the novel variation we observe in the classic 1–14 Ca^{2+}/CaM binding mode underscores the exceptionally adaptive nature of Ca^{2+}/CaM for target recognition.

Materials and Methods

Cloning, expression, and purification

Fragments of human Kv7.1–Kv7.5 (KCNQ1–KCNQ5) C-terminal domain were subcloned into either pSV272 (N. Pokala and T.M. Handel, unpublished results) or pET28-HMT vectors (Novagen) using NarI/HindIII or NdeI/HindIII sites. Both vectors contain the sequence for a hexahistidine tag followed by an MBP and a TEV protease site before the gene of interest. The only difference between the two vectors is that the NarI site following the TEV cleavage site in pSV272 is replaced by an NdeI site in pET28-HMT. Full-length native CaM and mutants were cloned into pEGST without an affinity tag as previously described.[72]

Kv7 fragments co-expressed with CaM in *E. coli* BL21(DE3)pLysS grown in 2YT media at 37 °C for 3 to 8 h. Cells containing constructs containing B–D segments were lysed by sonication in buffer containing 100 mM Tris (pH 8.8), 200 mM KCl, 10% sucrose, 1 mM $MgCl_2$, 1 mM PMSF, 20 μg ml^{-1} lysozyme, and 25 μg ml^{-1} DNase I. 1 mM $CaCl_2$ or 1 mM EGTA was also added before cell lysis depending on whether calcium-bound or calcium-free forms were the subject of purification. Lysed cells were centrifuged at 25,000***g*** for 30 min to remove insoluble material. For constructs spanning the A–D segments, the 10% sucrose in the lysis buffer was replaced by 10% glycerol and the cell lysis was performed using an Emulsiflex C-5 homogenizer (Avestin).

For all complexes, the soluble fraction containing the Kv7 fragment and CaM was purified on a Poros20MC (PerSeptive Biosystems) column equilibrated in buffer A (250 mM KCl, 1 mM $CaCl_2$, and 10 mM Hepes buffer, pH 7.4). When EGTA was used in the lysis buffer, a buffer of identical composition but lacking $CaCl_2$ replaced buffer A. After loading the sample, the column was washed in two steps: first using 3 column volumes of buffer A and then using 3 column volumes of buffer A plus 30 mM imidazole to remove weakly bound contaminants. Bound protein was then eluted using an imidazole gradient from 30 mM to 300 mM over 6 column volumes. After repeated spin concentration using a 50-kDa-cutoff Amicon Ultra-15 concentrator (Millipore) and dilution with buffer A to remove imidazole, the eluate from the Poros20MC column was loaded on to an amylose (New England Biolabs) column and washed with buffer A. The bound protein was then eluted in buffer A plus 10 mM maltose. The purified protein was digested with histidine-tagged TEV protease[73] in the amylose column elution buffer overnight at room temperature and was subsequently passed over a Poros20MC and amylose column run in buffer A plus 1 mM $CaCl_2$ to remove the protease and uncleaved material. Flow through was collected and concentrated using an Amicon Ultra-15 concentrator with a 10-kDa cutoff. During this process, the buffer was exchanged to a buffer of 10 mM KCl, 1 mM $CaCl_2$, and 10 mM Tris, pH 8.8, through a cycle of dilution and concentration. The sample was further purified using Resource Q or HiLoadQ (GE Healthcare) anion-exchange column and a gradient from 100 mM KCl to 350 mM KCl over 15 column volumes. This step is important for removal of residual His-MBP. The concentration of the purified complex was determined by measuring the absorption at 280 nm.[74]

Pull-down experiments

Various HMT-tagged Kv7 constructs were co-expressed with CaM as described above. Cells were lysed by sonication and centrifuged at 25,000***g*** for 30 min. The supernatant (500 μl) was incubated with the same amount of buffer A (250 mM KCl, 1 mM $CaCl_2$ or EGTA, and 10 mM Hepes, pH 7.4) and 500 μl of amylose resin and incubated for 30 min at 4 °C. The unbound proteins were washed out using three washes with 5 ml of buffer A. Bound proteins were eluted by buffer A plus 10 mM maltose and analyzed by SDS-PAGE.

Crystallization and data collection

The Ca^{2+}/CaM:Kv7.4 B–C complex, containing Kv7.4 residues 522–593, yielded crystals suitable for structural studies grown using hanging drop vapor diffusion from a drop containing equal volumes (1 μl each) of purified protein (~20 mg/ml) and a reservoir solution of 1.6 M ammonium sulfate, 0.2 M sodium citrate (pH 6.0), 0.1 M sodium tartrate, and 4% isopropanol. Rectangular rod-shaped crystals appeared in 1–3 weeks at room temperature. Crystals having this morphology diffracted to ~2.8 Å but suffered from high mosaicity, anisotropy, and a large unit cell. One crystal having hexagonal plate morphology appeared in the same conditions subsequent to a round of crystal harvesting from the well in which it grew. This crystal diffracted sufficiently to be used for structure determination. Mass spectrometry analysis revealed that the protein in this particular well had been cleaved C-terminal to residue 551, leaving only the B segment. In contrast, mass spectroscopy analysis of wells containing rod-shaped crystals showed the presence of the complete Kv7.4 BC construct. Diffraction data were collected from frozen crystals at beamline 12-2 (Stanford Synchrotron Radiation Lightsource) and were indexed and processed in the space group $P6_522$ using MOSFLM and SCALA in the CCP4 package.[75]

Structure determination

The structure was determined by a molecular replacement search using the N-lobe without calcium ions from the

sMLCK complex (PDB code: 1CDL) using PHASER.[76] Electron density indicating the Kv7.4 B-helix and Ca^{2+}/C-lobe was readily visible in the initial maps. Structure was built by iterative cycles of manual building and refinement using REFMAC[77] and PHENIX.[78] TLS refinement using three groups (Ca^{2+}/N-lobe, Ca^{2+}/C-lobe, and Kv7.4 helix) was added in the last few cycles. Residues 524–549 of Kv7.4 and all of CaM except for a few residues at the N-terminus and in the loop interdomain linker (residues 78–82) were resolved. Structural quality was evaluated using MolProbity.[79]

SEC and MALS-RI analysis

Purified Kv7.4 C-terminal domain:CaM complexes were run through either a Superdex200 10/300 GL or a Superdex75 HR column depending on the size of the complex. The columns were calibrated using at least four standard protein molecular mass markers (HMW and LMW calibration kits, GE Healthcare). The running buffer contained 250 mM KCl, 1 mM $CaCl_2$ or 1 mM EDTA, and 10 mM Hepes, pH 7.4. When EDTA was used, EDTA was added to the sample to a final concentration of 5 mM and the sample was incubated for 10 min before the run.

MALS-refractive index (RI) analysis[41,42] was performed using miniDAWN™ TREOS (LS) and Optilab® T-rEX™ (RI) (Wyatt Technology) for simultaneous detection of UV, RI, and MALS signals run in line with a Superdex200 10/300 GL or Superdex75 HR column in a buffer of 200 mM KCl, 1 mM $CaCl_2$, and 10 mM Hepes, pH 7.4, calibrated using 0.2 mg bovine serum albumin as an internal standard. ASTRA® 6 software package (Wyatt Technology) was used to compute protein molecular mass (Mw) and protein monodispersity (Mw/Mn) from the UV, RI, and MALS outputs.

Equilibrium sedimentation

Equilibrium sedimentation experiment was carried out at 4 ºC using a Beckman Optima XL-A analytical ultracentrifuge (Beckman Coulter). For the CaM:Q4AD complex, the buffer contained 250 mM KCl, 1 mM EDTA, and 10 mM Tris, pH 8.0. For the CaM:Q4BD complex, the buffer contained 1 mM $CaCl_2$ instead of EDTA. The purified protein was dialyzed overnight in the final buffer. The dialysis buffer was then used to dilute the protein to the intended concentration and as the reference cell sample. The data processing followed previously described procedures.[24] The molecular mass of the complex was obtained through a single exponential fit to the distribution of the complex over the radius.

Survey of Ca^{2+}/CaM 1–14 structures

Structures of the Ca^{2+}/CaM:Kv7.4 B-helix (4GOW) and Ca^{2+}/CaM:sMLCK (1CDL) 1–14 complexes were used as search queries using the DALI server[80] to identify similar Ca^{2+}/CaM complexes. Redundant structures were removed from the comparison and the remaining structures were aligned and manually examined to identify those using a 1–14 binding motif.

Accession numbers

Coordinates and structure factors have been deposited in the PDB with the following accession code: 4GOW.

Acknowledgements

This work was supported by grants from the National Institutes of Health (R01 DC007664) and the American Heart Association (0740019N) to D.L.M. and by a European Molecular Biology Organization long-term fellowship to A.T. We thank Rachel E. Gate and Susan Shim for excellent technical support, Felix Findeisen for helpful comments on the manuscript, and members of the Minor laboratory for support throughout these studies. D.L.M. is an American Heart Association Established Investigator.

Author Contributions. Q.X., A.C, A.T., and D.L.M. conceived the study. Q.X, A.C., and A.T. performed the experiments and analyzed data. D.L.M. analyzed data and provided guidance and support throughout. Q.X., A.C., A.T., and D.L.M. wrote the paper.

Conflict of Interest. The authors declare no conflict of interest.

Supplementary Data

Supplementary data to this article can be found online at http://dx.doi.org/10.1016/j.jmb.2012.11.023

Received 21 August 2012;
Received in revised form 14 November 2012;
Accepted 15 November 2012
Available online 23 November 2012

Keywords:
Kv7 (KCNQ) voltage-gated potassium channel;
calmodulin;
X-ray crystallography;
SEC-MALS;
channel modulation

† Q.X. and A.C. contributed equally to this work.

Present address: Q. Xu, Institute of Nuclear-Agricultural Sciences, Zhejiang University, 268 Kaixuan Road, 310029 Hangzhou, China.

Abbreviations used:
CaM, calmodulin; MBP, maltose binding protein; TEV, tobacco etch virus; EDTA, ethylenediaminetetraacetic acid; EGTA, ethylene glycol tetraacetic acid; GST, glutathione *S*-transferase; SEC, size-exclusion chromatography; MALS, multiangle light scattering; RI, refractive index; sMLCK, smooth muscle myosin light chain kinase; NEM, *N*-ethylmaleimide; PDB, Protein Data Bank.

References

1. Gutman, G. A., Chandy, K. G., Adelman, J. P., Aiyar, J., Bayliss, D. A., Clapham, D. E. *et al.* (2003). International Union of Pharmacology. XLI. Compendium of voltage-gated ion channels: potassium channels. *Pharmacol. Rev.* **55**, 583–586.
2. Jentsch, T. J. (2000). Neuronal KCNQ potassium channels: physiology and role in disease. *Nat. Rev. Neurosci.* **1**, 21–30.
3. Jespersen, T., Grunnet, M. & Olesen, S. P. (2005). The KCNQ1 potassium channel: from gene to physiological function. *Physiology (Bethesda)*, **20**, 408–416.
4. Delmas, P. & Brown, D. A. (2005). Pathways modulating neural KCNQ/M (Kv7) potassium channels. *Nat. Rev. Neurosci.* **6**, 850–862.
5. Wang, H.-S., Pan, Z., Shi, W., Brown, B. S., Wymore, R. S., Cohen, I. S. *et al.* (1998). KCNQ2 and KCNQ3 potassium channel subunits: molecular correlates of the M-Channel. *Science*, **282**, 1890–1893.
6. Hernandez, C. C., Zaika, O., Tolstykh, G. P. & Shapiro, M. S. (2008). Regulation of neural KCNQ channels: signalling pathways, structural motifs and functional implications. *J. Physiol.* **586**, 1811–1821.
7. Barhanin, J., Lesage, F., Guillemare, E., Fink, M., Lazdunski, M. & Romey, G. (1996). K_VLQT1 and IsK (minK) proteins associate to form the I_{Ks} cardiac potassium current. *Nature*, **384**, 78–80.
8. Sanguinetti, M. C., Curran, M. E., Zou, A., Shen, J., Spector, P. S., Atkinson, D. L. & Meating, M. T. (1996). Coassembly of K_VLQT1 and minK (IsK) proteins to form cardiac I_{Ks} potassium channel. *Nature*, **384**, 80–83.
9. Wang, Q., Curran, M. E., Splawski, I., Burn, T. C., Millholland, J. M., VanRaay, T. J. *et al.* (1996). Positional cloning of a novel potassium channel gene: KVLQT1 mutations cause cardiac arrhythmias. *Nat. Genet.* **12**, 17–23.
10. Brown, D. A. & Passmore, G. M. (2009). Neural KCNQ (Kv7) channels. *Br. J. Pharmacol.* **156**, 1185–1195.
11. Barrese, V., Miceli, F., Soldovieri, M. V., Ambrosino, P., Iannotti, F. A., Cilio, M. R. & Taglialatela, M. (2010). Neuronal potassium channel openers in the management of epilepsy: role and potential of retigabine. *Clin. Pharmacol.* **2**, 225–236.
12. Fritch, P. C., McNaughton-Smith, G., Amato, G. S., Burns, J. F., Eargle, C. W., Roeloffs, R. *et al.* (2010). Novel KCNQ2/Q3 agonists as potential therapeutics for epilepsy and neuropathic pain. *J. Med. Chem.* **53**, 887–896.
13. Wickenden, A. D. & McNaughton-Smith, G. (2009). Kv7 channels as targets for the treatment of pain. *Curr. Pharm. Des.* **15**, 1773–1798.
14. Soldovieri, M. V., Miceli, F. & Taglialatela, M. (2011). Driving with no brakes: molecular pathophysiology of Kv7 potassium channels. *Physiology (Bethesda)*, **26**, 365–376.
15. Maljevic, S., Wuttke, T. V. & Lerche, H. (2008). Nervous system KV7 disorders: breakdown of a subthreshold brake. *J. Physiol.* **586**, 1791–1801.
16. Yu, F. H., Yarov-Yarovoy, V., Gutman, G. A. & Catterall, W. A. (2005). Overview of molecular relationships in the voltage-gated ion channel superfamily. *Pharmacol. Rev.* **57**, 387–395.
17. Haitin, Y. & Attali, B. (2008). The C-terminus of Kv7 channels: a multifunctional module. *J. Physiol.* **586**, 1803–1810.
18. Wiener, R., Haitin, Y., Shamgar, L., Fernandez-Alonso, M. C., Martos, A., Chomsky-Hecht, O. *et al.* (2008). The KCNQ1 (Kv7.1) COOH terminus, a multitiered scaffold for subunit assembly and protein interaction. *J. Biol. Chem.* **283**, 5815–5830.
19. Gamper, N. & Shapiro, M. S. (2003). Calmodulin mediates Ca^{2+}-dependent modulation of M-type K^+ channels. *J. Gen. Physiol.* **122**, 17–31.
20. Ghosh, S., Nunziato, D. A. & Pitt, G. S. (2006). KCNQ1 assembly and function is blocked by long-QT syndrome mutations that disrupt interaction with calmodulin. *Circ. Res.* **98**, 1048–1054.
21. Shamgar, L., Ma, L., Schmitt, N., Haitin, Y., Peretz, A., Wiener, R. *et al.* (2006). Calmodulin is essential for cardiac IKS channel gating and assembly: impaired function in long-QT mutations. *Circ. Res.* **98**, 1055–1063.
22. Wen, H. & Levitan, I. B. (2002). Calmodulin is an auxiliary subunit of KCNQ2/3 potassium channels. *J. Neurosci.* **22**, 7991–8001.
23. Yus-Najera, E., Santana-Castro, I. & Villarroel, A. (2002). The identification and characterization of a noncontinuous calmodulin-binding site in noninactivating voltage-dependent KCNQ potassium channels. *J. Biol. Chem.* **277**, 28545–28553.
24. Howard, R. J., Clark, K. A., Holton, J. M. & Minor, D. L., Jr. (2007). Structural insight into KCNQ (Kv7) channel assembly and channelopathy. *Neuron*, **53**, 663–675.
25. Xu, Q. & Minor, D. L., Jr. (2009). Crystal structure of a trimeric form of the K(V)7.1 (KCNQ1) A-domain tail coiled-coil reveals structural plasticity and context dependent changes in a putative coiled-coil trimerization motif. *Protein Sci.* **18**, 2100–2114.
26. Soldovieri, M. V., Miceli, F., Bellini, G., Coppola, G., Pascotto, A. & Taglialatela, M. (2007). Correlating the clinical and genetic features of benign familial neonatal seizures (BFNS) with the functional consequences of underlying mutations. *Channels (Austin)*, **1**, 228–233.
27. Gardiner, M. (2006). Molecular genetics of infantile nervous system channelopathies. *Early Hum. Dev.* **82**, 775–779.
28. Singh, N. A., Westenskow, P., Charlier, C., Pappas, C., Leslie, J., Dillon, J. *et al.* (2003). KCNQ2 and KCNQ3 potassium channel genes in benign familial neonatal convulsions: expansion of the functional and mutation spectrum. *Brain*, **126**, 2726–2737.
29. Gamper, N., Li, Y. & Shapiro, M. S. (2005). Structural requirements for differential sensitivity of KCNQ K^+ channels to modulation by Ca^{2+}/calmodulin. *Mol. Biol. Cell*, **16**, 3538–3551.
30. Zaika, O., Tolstykh, G. P., Jaffe, D. B. & Shapiro, M. S. (2007). Inositol triphosphate-mediated Ca^{2+} signals direct purinergic P2Y receptor regulation of neuronal ion channels. *J. Neurosci.* **27**, 8914–8926.
31. Roden, D. M. (2006). A new role for calmodulin in ion channel biology. *Circ. Res.* **98**, 979–981.
32. Asada, K., Kurokawa, J. & Furukawa, T. (2009). Redox- and calmodulin-dependent S-nitrosylation of the KCNQ1 channel. *J. Biol. Chem.* **284**, 6014–6020.
33. Bal, M., Zaika, O., Martin, P. & Shapiro, M. S. (2008). Calmodulin binding to M-type K^+ channels assayed by TIRF/FRET in living cells. *J. Physiol.* **586**, 2307–2320.

34. Gomez-Posada, J. C., Aivar, P., Alberdi, A., Alaimo, A., Etxeberria, A., Fernandez-Orth, J. *et al.* (2011). Kv7 channels can function without constitutive calmodulin tethering. *PLoS One*, **6**, e25508.
35. Kharkovets, T., Hardelin, J. P., Safieddine, S., Schweizer, M., El-Amraoui, A., Petit, C. & Jentsch, T. J. (2000). KCNQ4, a K^+ channel mutated in a form of dominant deafness, is expressed in the inner ear and the central auditory pathway. *Proc. Natl Acad. Sci. USA*, **97**, 4333–4338.
36. Kubisch, C., Schroeder, B. C., Friedrich, T., Lütjohan, B., El-Amaraoui, A., Marlin, S. *et al.* (1999). KCNQ4, a novel potassium channel expressed in sensory outer hair cells, is mutated in dominant deafness. *Cell*, **96**, 437–446.
37. Heidenreich, M., Lechner, S. G., Vardanyan, V., Wetzel, C., Cremers, C. W., De Leenheer, E. M. *et al.* (2012). KCNQ4 K(+) channels tune mechanoreceptors for normal touch sensation in mouse and man. *Nat. Neurosci.* **15**, 138–145.
38. Minor, D. L., Jr. (2007). The neurobiologist's guide to structural biology: a primer on why macromolecular structure matters and how to evaluate structural data. *Neuron*, **54**, 511–533.
39. Laue, T. M. (1995). Sedimentation equilibrium as a thermodynamic tool. *Methods Enzymol.* **259**, 427–453.
40. Laue, T. M., Bhairavi, B. D., Ridgeway, T. M. & Pelletier, S. L. (1992). Computer-aided interpretation of analytical sedimentation data for proteins. In *Analytical Ultracentrifugation in Biochemistry and Polymer Science* (Harding, S. E., Rowe, A. J. & Horton, J. C., eds), Royal Society of Chemistry, Cambridge, UK.
41. Folta-Stogniew, E. & Williams, K. R. (1999). Determination of molecular masses of proteins in solution: implementation of an HPLC size exclusion chromatography and laser light scattering service in a core laboratory. *J. Biomol. Tech.* **10**, 51–63.
42. Folta-Stogniew, E. (2006). Oligomeric states of proteins determined by size-exclusion chromatography coupled with light scattering, absorbance, and refractive index detectors. *Methods Mol. Biol.* **328**, 97–112.
43. Maljevic, S., Lerche, C., Seebohm, G., Alekov, A. K., Busch, A. E. & Lerche, H. (2003). C-terminal interaction of KCNQ2 and KCNQ3 K^+ channels. *J. Physiol.* **548**, 353–360.
44. Schwake, M., Athanasiadu, D., Beimgraben, C., Blanz, J., Beck, C., Jentsch, T. J. *et al.* (2006). Structural determinants of M-type KCNQ (Kv7) K^+ channel assembly. *J. Neurosci.* **26**, 3757–3766.
45. Schwake, M., Jentsch, T. J. & Friedrich, T. (2003). A carboxy-terminal domain determines the subunit specificity of KCNQ K^+ channel assembly. *EMBO Rep.* **4**, 76–81.
46. Meador, W. E., Means, A. R. & Quiocho, F. A. (1992). Target enzyme recognition by calmodulin: 2.4 Å structure of a calmodulin-peptide complex. *Science*, **257**, 1251–1255.
47. Rhoads, A. R. & Friedberg, F. (1997). Sequence motifs for calmodulin recognition. *Biochem. J.* **11**, 331–340.
48. Hoeflich, K. P. & Ikura, M. (2002). Calmodulin in action: diversity in target recognition and activation mechanisms. *Cell*, **108**, 739–742.
49. Ikura, M., Barbato, G., Klee, C. B. & Bax, A. (1992). Solution structure of calmodulin and its complex with a myosin light chain kinase fragment. *Cell Calcium*, **13**, 391–400.
50. Maljevic, S., Wuttke, T. V., Seebohm, G. & Lerche, H. (2010). KV7 channelopathies. *Pflugers Arch.* **460**, 277–288.
51. Schmitt, N., Calloe, K., Nielsen, N. H., Buschmann, M., Speckmann, E. J., Schulze-Bahr, E. & Schwarz, M. (2007). The novel C-terminal KCNQ1 mutation M520R alters protein trafficking. *Biochem. Biophys. Res. Commun.* **358**, 304–310.
52. Moulard, B., Picard, F., le Hellard, S., Agulhon, C., Weiland, S., Favre, I. *et al.* (2001). Ion channel variation causes epilepsies. *Brain Res. Brain Res. Rev.* **36**, 275–284.
53. Borgatti, R., Zucca, C., Cavallini, A., Ferrario, M., Panzeri, C., Castaldo, P. *et al.* (2004). A novel mutation in KCNQ2 associated with BFNC, drug resistant epilepsy, and mental retardation. *Neurology*, **63**, 57–65.
54. Larsen, L. A., Fosdal, I., Andersen, P. S., Kanters, J. K., Vuust, J., Wettrell, G. & Christiansen, M. (1999). Recessive Romano–Ward syndrome associated with compound heterozygosity for two mutations in the KVLQT1 gene. *Eur. J. Hum. Genet.* **7**, 724–728.
55. Li, Y., Gamper, N. & Shapiro, M. S. (2004). Single-channel analysis of KCNQ K^+ channels reveals the mechanism of augmentation by a cysteine-modifying reagent. *J. Neurosci.* **24**, 5079–5090.
56. Roche, J. P., Westenbroek, R., Sorom, A. J., Hille, B., Mackie, K. & Shapiro, M. S. (2002). Antibodies and a cysteine-modifying reagent show correspondence of M current in neurons to KCNQ2 and KCNQ3 K^+ channels. *Br. J. Pharmacol.* **137**, 1173–1186.
57. Aoyagi, M., Arvai, A. S., Tainer, J. A. & Getzoff, E. D. (2003). Structural basis for endothelial nitric oxide synthase binding to calmodulin. *EMBO J.* **22**, 766–775.
58. De Diego, I., Kuper, J., Bakalova, N., Kursula, P. & Wilmanns, M. (2010). Molecular basis of the death-associated protein kinase-calcium/calmodulin regulator complex. *Sci. Signal.* **3**, ra6.
59. Xia, C., Misra, I., Iyanagi, T. & Kim, J. J. (2009). Regulation of interdomain interactions by calmodulin in inducible nitric-oxide synthase. *J. Biol. Chem.* **284**, 30708–30717.
60. Ataman, Z. A., Gakhar, L., Sorensen, B. R., Hell, J. W. & Shea, M. A. (2007). The NMDA receptor NR1 C1 region bound to calmodulin: structural insights into functional differences between homologous domains. *Structure*, **15**, 1603–1617.
61. Sarhan, M. F., Tung, C. C., Van Petegem, F. & Ahern, C. A. (2012). Crystallographic basis for calcium regulation of sodium channels. *Proc. Natl Acad. Sci. USA*, **109**, 3558–3563.
62. Zhang, M., Abrams, C., Wang, L., Gizzi, A., He, L., Lin, R. *et al.* (2012). Structural basis for calmodulin as a dynamic calcium sensor. *Structure*, **20**, 911–923.
63. Schumacher, M. A., Rivard, A. F., Bächinger, H. P. & Adelman, J. P. (2001). Structure of the gating domain of a Ca^{2+} activatived K^+ channel complexed with Ca^{2+}/calmodulin. *Nature*, **410**, 1120–1124.

64. Feldkamp, M. D., Yu, L. & Shea, M. A. (2011). Structural and energetic determinants of apo calmodulin binding to the IQ motif of the Na(V)1.2 voltage-dependent sodium channel. *Structure*, **19**, 733–747.
65. Chagot, B. & Chazin, W. J. (2011). Solution NMR structure of Apo-calmodulin in complex with the IQ motif of human cardiac sodium channel NaV1.5. *J. Mol. Biol.* **406**, 106–119.
66. Schumacher, M. A., Crum, M. & Miller, M. C. (2004). Crystal structures of apocalmodulin and an apocalmodulin/SK potassium channel gating domain complex. *Structure*, **12**, 849–860.
67. Bai, C. X., Namekata, I., Kurokawa, J., Tanaka, H., Shigenobu, K. & Furukawa, T. (2005). Role of nitric oxide in Ca^{2+} sensitivity of the slowly activating delayed rectifier K^+ current in cardiac myocytes. *Circ. Res.* **96**, 64–72.
68. Hernandez, C. C., Zaika, O. & Shapiro, M. S. (2008). A carboxy-terminal inter-helix linker as the site of phosphatidylinositol 4,5-bisphosphate action on Kv7 (M-type) K^+ channels. *J. Gen. Physiol.* **132**, 361–381.
69. Xu, T., Nie, L., Zhang, Y., Mo, J., Feng, W., Wei, D. *et al.* (2007). Roles of alternative splicing in the functional properties of inner ear-specific KCNQ4 channels. *J. Biol. Chem.* **282**, 23899–23909.
70. Shahidullah, M., Santarelli, L. C., Wen, H. & Levitan, I. B. (2005). Expression of a calmodulin-binding KCNQ2 potassium channel fragment modulates neuronal M-current and membrane excitability. *Proc. Natl Acad. Sci. USA*, **102**, 16454–16459.
71. Etxeberria, A., Aivar, P., Rodriguez-Alfaro, J. A., Alaimo, A., Villace, P., Gomez-Posada, J. C. *et al.* (2008). Calmodulin regulates the trafficking of KCNQ2 potassium channels. *FASEB J.* **22**, 1135–1143.
72. Van Petegem, F., Chatelain, F. C. & Minor, D. L., Jr. (2005). Insights into voltage-gated calcium channel regulation from the structure of the CaV1.2 IQ domain-Ca^{2+}/calmodulin complex. *Nat. Struct. Mol. Biol.* **12**, 1108–1115.
73. Kapust, R. B., Tozser, J., Fox, J. D., Anderson, D. E., Cherry, S., Copeland, T. D. & Waugh, D. S. (2001). Tobacco etch virus protease: mechanism of autolysis and rational design of stable mutants with wild-type catalytic proficiency. *Protein Eng.* **14**, 993–1000.
74. Edelhoch, H. (1967). Spectroscopic determination of tryptophan and tyrosine in proteins. *Biochemistry*, **6**, 1948–1954.
75. Collaborative Computational Project, No. 4 (1994). The CCP4 suite: programs for protein crystallography. *Acta Crystallogr., Sect. D: Biol. Crystallogr.* **50**, 760–763.
76. Storoni, L. C., McCoy, A. J. & Read, R. J. (2004). Likelihood-enhanced fast rotation functions. *Acta Crystallogr., Sect. D: Biol. Crystallogr.* **60**, 432–438.
77. Murshudov, G. N., Vagin, A. A. & Dodson, E. J. (1997). Refinement of macromolecular structures by the maximum-likelihood method. *Acta Crystallogr., Sect. D: Biol. Crystallogr.* **53**, 240–255.
78. Adams, P. D., Afonine, P. V., Bunkoczi, G., Chen, V. B., Davis, I. W., Echols, N. *et al.* (2010). PHENIX: a comprehensive Python-based system for macromolecular structure solution. *Acta Crystallogr., Sect. D: Biol. Crystallogr.* **66**, 213–221.
79. Chen, V. B., Arendall, W. B., 3rd, Headd, J. J., Keedy, D. A., Immormino, R. M., Kapral, G. J. *et al.* (2010). MolProbity: all-atom structure validation for macromolecular crystallography. *Acta Crystallogr., Sect. D: Biol. Crystallogr.* **66**, 12–21.
80. Holm, L. & Rosenstrom, P. (2010). Dali server: conservation mapping in 3D. *Nucleic Acids Res.* **38**, W545–W549.

25 February 2013

Supplementary material for

Structure of a Ca^{2+}/CaM:Kv7.4 (KCNQ4) B helix complex provides insight into M-current modulation

Qiang Xu*[1,5], Aram Chang*[1], Alexandra Tolia[1], and Daniel L. Minor, Jr.[1,2,3,4,†]

[1] Cardiovascular Research Institute

[2] Departments of Biochemistry and Biophysics, and Cellular and Molecular Pharmacology

[3] California Institute for Quantitative Biosciences

University of California, San Francisco, CA 94158-2330

[4]Physical Biosciences

Lawrence Berkeley National Laboratory

Berkeley, CA 94720 USA

[5]Present address:

Institute of Nuclear-Agricultural Sciences

268 Kaixuan Road

Zhejiang University

310029 Hangzhou

China

25 February 2013

Figure S1

Xu *et al.*

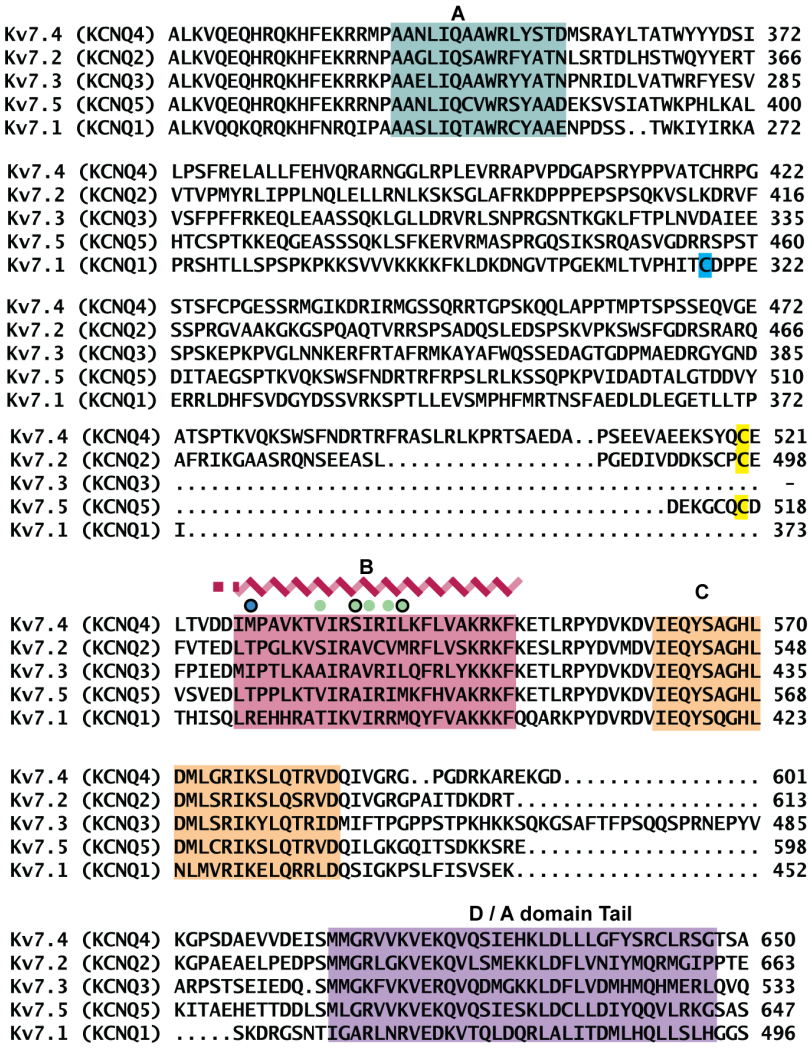

Figure S1 Kv7 C-terminal tail sequence alignment Sequence alignment of cytoplasmic C-terminal tails of human Kv7.4 AAD14680, residues 323-650; human Kv7.2 CAH72962.1, residues 317-663; human Kv7.3 NP_001191753.1, residues 236-653; human Kv7.5 NP_001153604.1, residues 351-647; human Kv7.1 CAB44650.1 residues 225-452. A, B, C, and D regions are dark green, red, orange, and purple, respectively. Secondary structure of the B-segment is indicated. Blue and green circles indicate Ca^{2+}/N-lobe and Ca^{2+}/C-lobe anchors, respectively. Open black circles indicate the 1-10-14 motif. Filled grey and black circles under the B-segments indicate the two suggested 1-5-10 motifs from Yus-Najera *et al.*[1]. Yellow and blue indicates C-terminal tail cysteines reactive to NEM[2] and S-nitrosylation[3], respectively.

Figure S2

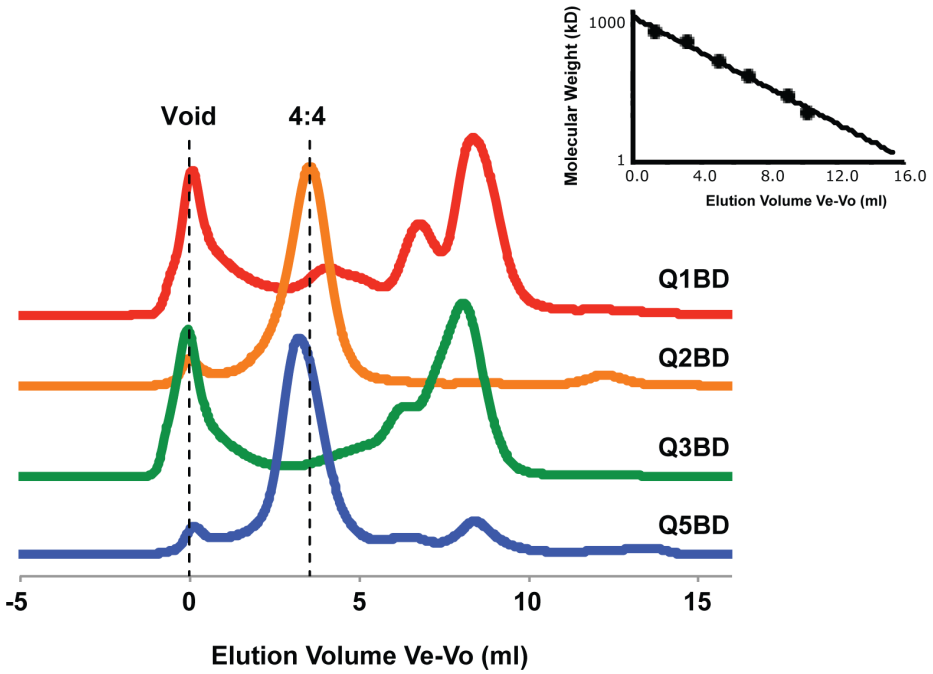

Figure S2 Size exclusion chromatography of Ca^{2+}/CaM:BD complexes from Kv7 isoforms Superdex200 (Amersham Biosciences) chromatography normalized absorbance profiles for Ca^{2+}/CaM:HMT-BD complexes from Kv7.1 (Q1BD, red), Kv7.2 (Q2BD, orange), Kv7.3 (Q3BD, green) and Kv7.5 (Q5BD, blue). Vertical dashed lines indicate the void volume and the expected elution volumes of 4:4 complexes based on the standard curve (inset). Expected sizes of a 4:4 Ca^{2+}/CaM:HMT-BD complexes for each construct are: Ca^{2+}/CaM:HMT-Q1BD, 302.0 kD; Ca^{2+}/CaM:HMT-Q2, 303.2 kD; Ca^{2+}/CaM:HMT-Q3BD, 317.6 kD; Ca^{2+}/CaM:HMT-Q5BD: 302.8 kD).

25 February 2013

Figure S3

Xu *et al.*

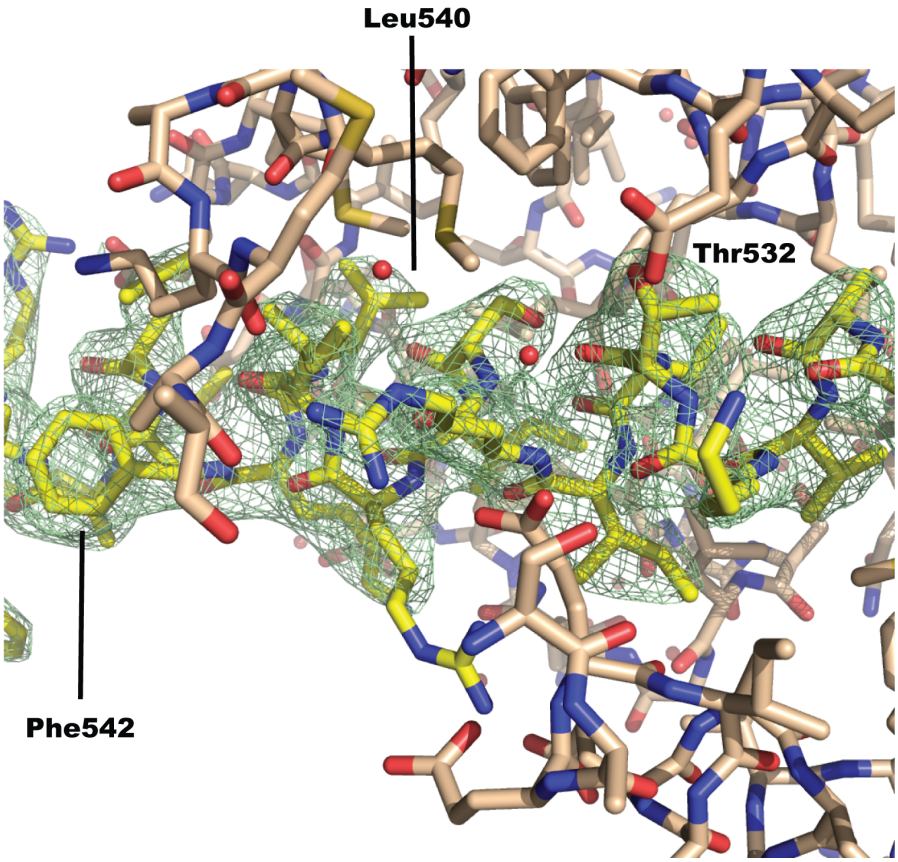

Figure S3 Weighted 2Fo-Fc electron density for the Kv7.4 B-helix contoured at 1.2σ. Model shows the final refined structure. Ca^{2+}/CaM is tan. Kv7.4 B-helix is bright yellow. Nitrogen, oxygen, and sulfur atoms are colored blue, red, and yellow respectively. Select Kv7.4 B-helix residues are labeled.

Figure S4 **Xu *et al.***

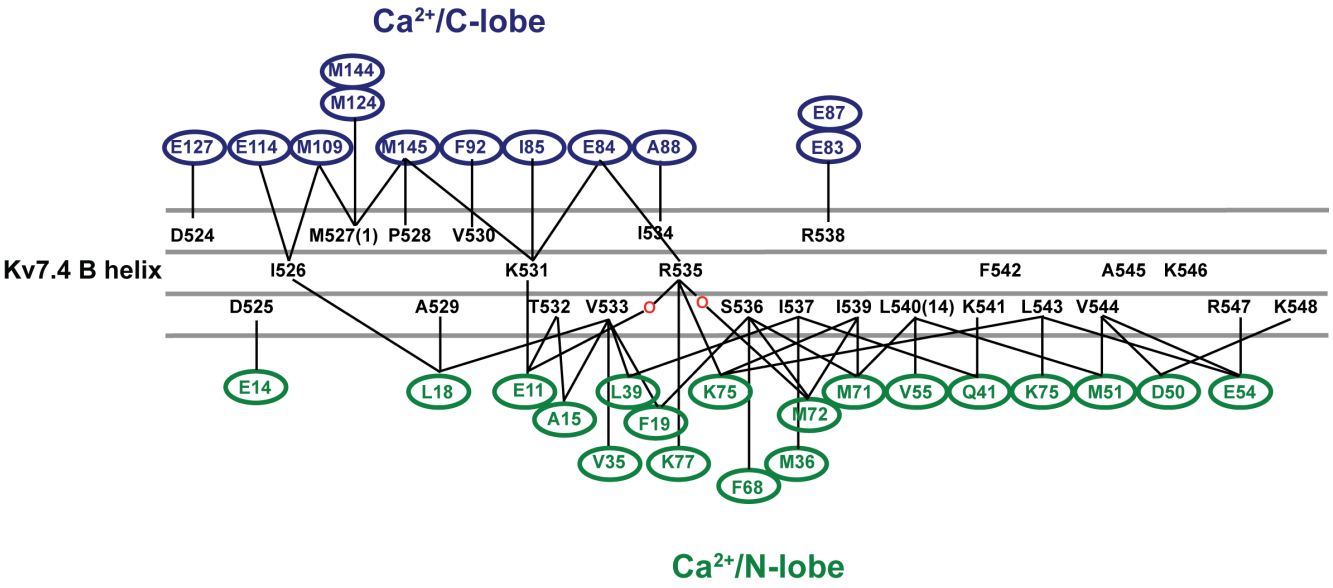

Figure S4 Schematic of Ca^{2+}/CaM Kv7.4 B-helix contacts Residues making contacts, ≤ 4Å, to Ca^{2+}/C-lobe and Ca^{2+}/N-lobe alone are shown in the top and bottom rows, respectively. Central row includes residues contacting both lobes, or with no contacts to either lobe. Positions 1 and 14 of the 1-14 motif are indicated in parentheses. Water-mediated contacts are indicted by the red 'o'. K548-D50 interaction is 4.2Å.

Figure S5

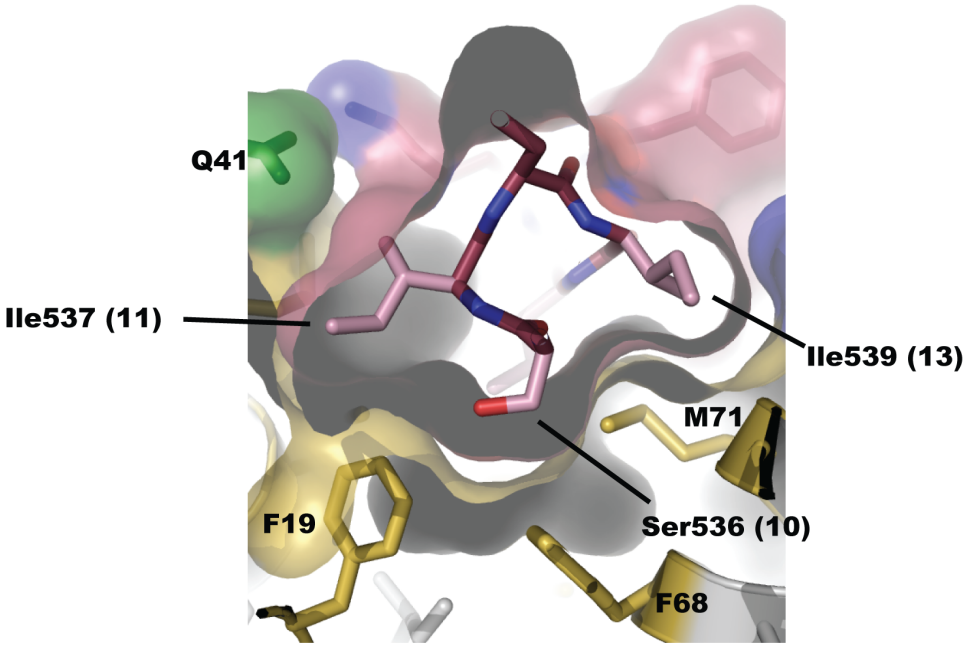

Figure S5 Environment of Kv7.4 (KCNQ4) Ser536 Cutaway view showing the buried environment and surfaces surrounding Kv7.4 Ser536, position (10). Kv7.4 B helix is shown as sticks and colored firebrick with nitrogen and oxygen atoms are colored blue and red, respectively. Kv7.4 anchor sidechains are pink. Hydrophobic, basic, acidic, and polar sidechains from CaM are colored yellow, blue, red, and green, respectively. Key residues of Ca^{2+}/CaM are labeled by single letter code. Kv7.4 B-helix residues are labeled in three letter code followed by the position number within the 1-14 motif, indicated in parenthesis.

PDB ID	(1) position	Target origin
1CDL	W	Chicken smooth muscle myosin light chain kinase
2BBM	W	Skeletal muscle myosin light chain kinase
1NIW	F	Endothelial nitric oxide synthase peptide
2O60	F	Neuronal nitric oxide synthase
3HR4	L	Human inducible nitric oxide synthase
1YR5	W	Human death-associated protein kinase 1
2Y4V	Y	Human death-associated protein kinase 1 ((1) position mutant of 1YR5)
1WRZ	W	Human death-associated protein kinase 2
2FOT	W	AlphaII-spectrin
1MXE	W	Calmodulin kinase I
4AXR	W	*A. thaliana* plasma-membrane Ca^{2+}-ATPase

Supplementary Table 1

Table of 1-14 Ca^{2+}/CaM structures showing: PDB codes, identity of residue at the (1) position of the 1-14 motif, and target origin.

25 February 2013

Supplementary References

1. Yus-Najera, E., Santana-Castro, I. & Villarroel, A. (2002). The Identification and Characterization of a Noncontinuous Calmodulin-binding Site in Noninactivating Voltage-dependent KCNQ Potassium Channels. *J Biol Chem* 277, 28545-53.
2. Gamper, N., Li, Y. & Shapiro, M. S. (2005). Structural requirements for differential sensitivity of KCNQ K+ channels to modulation by Ca2+/calmodulin. *Mol Biol Cell* 16, 3538-51.
3. Asada, K., Kurokawa, J. & Furukawa, T. (2009). Redox- and calmodulin-dependent S-nitrosylation of the KCNQ1 channel. *J Biol Chem* 284, 6014-20.